ABSTRACT

Title of Thesis: UNDERSTANDING THE CONTRIBUTION OF THE CENTRAL EXTENDED AMYGDALA TO DISPOSITIONAL NEGATIVITY

Rachael M. Tillman, Master of Science, 2017

Thesis Directed By: Dr. Alexander J. Shackman, Assistant Professor
Department of Psychology

Dispositional negativity (DN) is a key risk factor for a spectrum of adverse outcomes, including anxiety disorders, depression, and comorbid substance abuse. The central extended amygdala (EAc; an anatomical concept encompassing the bed nucleus of the stria terminalis [BST] and central nucleus of the amygdala [Ce]) is implicated in the development and maintenance of these disorders. However, disorders, like other psychological processes, reflect the coordinated actions of widely distributed networks. Yet, the functional architecture of the human EAc and its relation to individual differences in DN remains poorly understood.

We investigated intrinsic functional connectivity (iFC) of the EAc in 185 healthy adults. Whole-brain regression analyses revealed that the BST and Ce show iFC with one another via the sublenticular extended amygdala. While both regions showed significant iFC with the ventromedial prefrontal cortex and with cingulate territories involved in adaptive control of anxiety-related behavior, the BST showed more robust coupling. Contrary to expectations, EAc iFC was not significantly associated with individual differences in DN. These observations provide a novel neurobiological framework for understanding a range of stress-sensitive disorders.

UNDERSTANDING THE CONTRIBUTION OF THE CENTRAL EXTENDED AMYGDALA TO DISPOSITIONAL NEGATIVITY

by

Rachael M. Tillman

Thesis submitted to the Faculty of the Graduate School of the
University of Maryland, College Park, in partial fulfillment
of the requirements for the degree of
Master of Science
2017

Advisory Committee:
Professor Alexander J. Shackman, Chair
Professor Nathan A. Fox
Professor Luiz Pessoa
Professor Elizabeth Redcay

Acknowledgements

I am deeply grateful to my mentors, Dr. Alexander Shackman and Dr. Jason Smith, for their guidance and support throughout this project and my research training. I would also like to express my gratitude to my Master's Thesis committee: Drs. Fox, Pessoa, and Redcay. Your feedback and guidance has been crucial for both the development of this project and my development as a researcher. I am especially grateful to Dr. Salavatore Torrisi, Dr. Brendon Nacewicz, and Dr. Jennifer Blackford for their consultation and their efforts in creating seed regions for my project. Finally, I would like to thank my laboratory teammates, Melissa Stockbridge, Claire Kaplan, and Kathryn DeYoung, for their support and aid in data organization.

Table of Contents

Acknowledgements ii
Table of Contents iii
List of Tables iv
List of Figures v
Chapter 1: Introduction 1
Chapter 2: Methods 9
Chapter 3: Results 15
Chapter 4: Discussion 17
Tables 23
Figures 32
Supplementary Figures 43
References 47

List of Tables

Table 1. Sample demographics.

Table 2. Regions showing significant functional connectivity with the BST.

Table 3. Regions showing significant functional connectivity with the Ce.

Table 4. Regions showing significant functional connectivity with both the BST and Ce.

Table 5. Regions showing significant differences in functional connectivity between the BST and Ce

List of Figures

Figure 1. Primate central extended amygdala.

Figure 2. Structural connections of the central extended amygdala.

Figure 3. Bed Nucleus of the Stria Terminalis (BST) and Central Nucleus of the Amygdala (Ce) Seeds.

Figure 4. Basal Regions Showing Significant Functional Connectivity with the Bed Nucleus of the Stria Terminalis (BST) and Central Nucleus of the Amygdala (Ce).

Figure 5. The Bed Nucleus of the Stria Terminalis (BST) and Central Nucleus of the Amygdala (Ce) are Functionally Linked via the Sublenticular Extended Amygdala (SLEA).

Figure 6. Basal Regions Showing Differential Functional Connectivity with the Bed Nucleus of the Stria Terminalis (BST) and Central Nucleus of the Amygdala (Ce).

Figure 7. Cortical Regions Showing Significant Functional Connectivity with the Bed Nucleus of the Stria Terminalis (BST), Central Nucleus of the Amygdala (Ce), or Both.

List of Supplementary Figures

Supplementary Figure 1. Individual differences in dispositional negativity for subjects with usable imaging data (n =130)

Supplementary Figure 2. Jülich Centromedial Amygdala (CM) Seeds.

Supplementary Figure 3. Confirmatory Analysis of the Default Mode Network (DMN).

Supplementary Figure 4. Exploratory comparison of the intrinsic functional connectivity of the Ce and CM seeds.

Chapter 1: Introduction

Dispositional negativity (i.e., negative emotionality), the tendency to experience and express more frequent, intense, or enduring negative affect, is a trait-like phenotype that first emerges early in development, persists into adulthood, and reflects a combination of heritable and non-heritable factors (Shackman et al., 2016a). It is a broad dimension that subsumes individual differences in anxiety sensitivity, behavioral inhibition, harm avoidance, neuroticism, and trait anxiety (Barlow, Sauer-Zavala, Carl, Bullis, & Ellard, 2013; Caspi, Roberts, & Shiner, 2005). There is clear evidence that elevated levels of dispositional negativity confer increased risk for a broad spectrum of adverse outcomes, including anxiety disorders, depression, and co-occuring substance abuse (e.g., Kotov, Gamez, Schmidt, & Watson, 2010; Ormel et al., 2013; Zinbarg et al., 2016). These debilitating neuropsychiatric disorders are common, burdensome, and challenging to treat (Bystritsky, 2006; Kessler, Petukhova, Sampson, Zaslavsky, & Wittchen, 2012; Whiteford et al., 2013), underscoring the need to develop a deeper understanding of the neural circuits supporting individual differences in dispositional negativity.

Work in rodents, monkeys, and humans suggests that the central extended amygdala—an anatomical concept encompassing the bed nucleus of the stria terminalis (BST) and the neighboring central nucleus of the amygdala (Ce) (Alheid & Heimer, 1988)—is a key substrate for individual differences in dispositional negativity (**Figure 1**; Shackman et al., 2016a; Shackman & Fox, 2016). As shown in **Figure 2,** the BST and Ce are structurally connected in humans and other primates via two major fiber bundles, the ventral amygdalofugal pathway and the stria

terminalis (Johnston, 1923; Nauta, 1961; Yilmazer-Hanke, 2012). From the Ce, the ventral amygdalofugal pathway courses forward and medially, passing through the sublenticular extended amygdala (SLEA), a bridge of neurons harbored within the substantia innominata. Recent tracing studies suggest that the SLEA represents a key structural hub for communications between the BST and Ce (Ce ↔ SLEA ↔ BST; Oler et al., 2016).

Large-scale imaging studies in monkeys indicate that metabolism in the BST and the Ce is associated with elevated levels of dispositional negativity (Fox et al., 2015a); Shackman, Fox, Oler, Shelton, Davidson, & Kalin, 2013). Likewise, imaging studies in humans demonstrate that the dorsal amygdala, in the region of the Ce, is more reactive in adults with elevated levels of dispositional negativity (Calder, Ewbank, & Passamonti, 2011; Schulyer et al., 2014) with a childhood history of elevated behavioral inhibition (Fox & Kalin, 2014) and with anxiety disorders (Etkin & Wager, 2007).

Mechanistic work in monkeys and rodents suggests that the Ce plays a causal role in the momentary expression of fear and anxiety (Shackman & Fox, 2016). In monkeys, for example, selective excitotoxic lesions of the Ce markedly attenuate signs of anxiety (e.g., freezing) elicited by potential threat (Kalin, Shelton, & Davidson, 2004). Conversely, manipulations that increase Ce metabolism in monkeys (i.e., via viral vector-mediated overexpression of corticotrophin-releasing hormone) potentiate threat-elicited defensive responses (Kalin et al., 2016). Broadly similar findings have been reported for human patients with circumscribed amygdala damage. Patient S.M., who has near-complete bilateral destruction of the amygdala,

shows a lack of negative affect in response to a range of aversive exteroceptive stimuli (e.g., frightening movies, haunted houses, snakes, spiders). She also reports abnormally low scores of dispositional negativity on common psychometric measures (Feinstein, Adolphs, Damasio, & Tranel, 2011; Feinstein, Adolphs, & Tranel, 2016; Tranel, Gullickson, Kock, & Adolphs, 2006).

Although the BST has been scrutinized much less intensely, recent experimental work in rodents motivates the hypothesis that this region plays a role broadly similar to that of the Ce (Calhoon & Tye, 2015; Shackman & Fox, 2016). Likewise, recent imaging studies demonstrate that the BST shows sustained levels of heightened activity in response to uncertain threat among humans and monkeys with a more negative disposition (Somerville, Whalen, & Kelley, 2010; Shackman et al., *in press*) and patients with anxiety disorders (Morey et al., 2009, Yassa, Hazlett, Stark, & Hoehn-Saric, 2012; Münsterkötter et al., 2015).

There is general consensus that dispositional negativity, like other psychological processes (Pessoa, 2013; Shackman, Fox, & Seminowicz, 2015), reflects the coordinated activity of distributed neural networks rather than isolated brain regions (Shackman et al., 2016a). Indeed, invasive anatomical tracing studies in primates show that the BST and Ce are embedded within a complex web of mono- and polysynaptically connected brain regions (Figure 1) (Freese & Amaral, 2009; Oler, et al., 2016). This structural foundation includes subcortical regions, like the periaqueductal gray (PAG), that trigger specific defensive responses (e.g., freezing and other forms of passive avoidance) to threat across mammalian species (Bandler, Price, & Keay, 2000; Nashold, Wilson, & Slaughter, 1969; Satpute et al., 2013).

Evidence from these tracing studies also suggest that a number of cortical regions including the anterior insula (aIns; Fox et al., 2015a), dorsolateral prefrontal cortex (dlPFC; Birn et al., 2014), mid-cingulate cortex (MCC; Shackman et al., 2011; Cavanagh & Shackman, 2015), and orbitofrontal cortex (OFC; Fox et al., 2010, 2015a; Kalin et al., 2016; Ogur & Price, 2000) are connected to central extended amygdala via polysynaptic structural pathways. Activity in these regions has been associated with individual differences in dispositional negativity and have been implicated in the adaptive regulation of fear, anxiety, and other aversive states in humans and monkeys (Shackman et al., 2016a).

Yet, the *functional* architecture of the BST and Ce networks in humans and their relevance to individual differences in dispositional negativity remain poorly understood. This partially reflects the fact that the BST and the Ce are small, heterogeneous structures that are challenging to identify using standard T1-weighted (T1w) magnetic resonance imaging. Furthermore, functional networks need not recapitulate the direct structural connections revealed by traditional tract tracing techniques (Pessoa, 2013). In fact, there is mounting evidence that regulatory signals can flow across more complex, indirect pathways (Ekstrom, Roelfsema, Arsenault, Bonmassar, & Vanduffel, 2008), and that robust functional connectivity exists between regions that lack direct structural connections (Birn et al., 2014; Honey et al., 2009; Lu et al., 2011; Vincent et al. 2007).

Recently, researchers have begun mapping the intrinsic (i.e., 'resting-state') functional connectivity of the BST (Avery, Clauss, Winder, Woodword, Heckers, & Blackford, 2014; Motzkin et al., 2015; Torrisi et al., 2015). fMRI-derived measures of

intrinsic functional connectivity are particularly useful for characterizing functional networks of the human BST and Ce as an noninvasive approach that is sensitive to functional networks extending across polysynaptic circuits (Buckner, Krienen, & Yeo, 2013). Results are generally consistent with what is known from invasive anatomical tracing studies in rodents (Dong & Swason, 2005; Heimer et al., 2007) and more limited work in nonhuman primates (Oler et al., *in press*), revealing robust functional connectivity between the BST and the amygdala, hippocampus, hypothalamus, caudate, thalamus, PAG, and cortical areas such as the precuneus, and ventromedial prefrontal cortex (vmPFC). Although a number of these regions are implicated in the pathophysiology of anxiety and addiction disorders (e.g., Fox et al., 2015b; Avery, Clauss & Blackford, 2016; Shackman & Fox, 2016), no study to date has looked the functional connectivity of the BST and its relevance to dispositional negativity. Furthermore, no study has examined both BST and Ce in the same sample, which would provide an important first opportunity to compare their functional networks.

Although several groups have investigated the intrinsic functional connectivity of the human amygdala, only a few studies have examined the connectivity patterns of the amygdala subdivisions (e.g., Roy et al., 2009) and their relevance to facets of dispositional negativity (e.g., behavioral inhibition; Baur et al., 2013; Blackford et al., 2014; Etkin et al., 2009; Roy et al., 2013; 2014). Importantly, nearly all of these studies relied on seeds derived from the histologically-derived Jülich probabilistic atlas (Amunts et al., 2005), which includes basolateral amygdala (BLA), centromedial amygdala (CMA), and superficial amygdala (SF) sub-regions. While the Jülich

probabilistic atlas (Amunts et al., 2005) achieves finer precision in characterizing the differing regions of the amygdala compared to whole-amygdala seeds, the atlas does not differentiate the Ce from other subnuclei regions such as the medial nucleus and anterior amygdala area. Furthermore, a number of investigators have reported that CMA seed is poorly registered to widely used brain templates (e.g., MNI152) and, as a consequence, includes voxels located in neighboring regions of the striatum (Entis, Doerga, Barrett, & Dickerson, 2012; Prèvost, McCabe, Jessup, Bossaerts, & O'Dohert, 2011; Hyrbouski et al., 2016). A more anatomically precise Ce seed is necessary to clarify existing models of amygdala subdivision function and to extend findings from mechanistic work in nonhuman primates. To date, only two studies have assessed the intrinsic functional connectivity of the Ce in humans. Oler and colleagues (2012) assessed Ce connectivity in a sample of healthy youth and reported robust coupling between the Ce and BST, striatum, cingulate, and temporal lobe. Results from Birn and colleagues (2014) reported a targeted analysis of Ce-PFC functional connectivity in a sample of pediatric anxiety patients. They observed that the Ce shows reduced functional connectivity with the Ce in patients relative to controls, consistent with evidence of reduced Ce-dlPFC connectivity in monkeys with a more anxious temperament (Birn et al., 2014).

To extend this body of work and address critical gaps in the literature, we harnessed the enhanced resolution afforded by multi-band fMRI (2-mm^3) to first trace the intrinsic functional connectivity of the BST and the Ce in 130 community-dwelling adults and then to identify the subset of functional connections most relevant to individual differences in dispositional negativity. We leveraged cutting-edge

techniques for data registration (boundary based registration; BBR) and normalization (SyN/ANTS), rigorous procedures for artifact correction as well as manual quality assurance, and maintained spatially unsmoothed data to further enhance spatial resolution and anatomical specificity. In addition, we utilized a recently developed probabilistic BST seed (Theiss, Ridgewell, McHugo, Heckers, & Blackford, 2016) and an anatomically precise Ce seed defined on a high-resolution (0.7mm), multi-modal probabilistic template for our main analyses. In addition, we also assessed, on an exploratory basis, the intrinsic functional connectivity of the more widely used Jülich CMA seed.

Based on prior work from Avery and colleagues (2014), Motzkin and colleagues (2015), and Torrisi and colleagues (2015), we predict our sample will yield a broadly similar pattern of BST functional connectivity. Subcortically, anticipated significant coupling between the BST and amygdala, SLEA, basal ganglia (i.e., accumbens, caudate, putamen, and pallidum), hypothalamus, hippocampus, PAG, and thalamus. Cortically, we anticipated significant coupling with regions along the midline (pregenual and posterior cingulate and precuneus) as well as lateral PFC (i.e., superior, medial, and inferior frontal gyri) and calcarine cortex.

Despite the limited intrinsic functional connectivity studies focusing on the human Ce, recent work in related areas does inform our study hypotheses. Specifically, we anticipated results similar to those reported by Birn et al. (2014) and Oler et al. (2012). We predicted significant coupling between the Ce and BST and dlPFC as well as pregenual and subgenual cingulate. Finally, based on studies investigating the functional connectivity of the centromedial amygdala subdivision

and facets of dispositional negativity (Blackford et al., 2014; Roy et al., 2013; 2014) and Birn and colleagues' findings in pediatric anxiety patients (2014), we anticipated that functional connectivity with regions involved in effortful regulation (e.g., dlPFC [including dorsal ACC/anterior MCC] and rostral and subgenual ACC) will be associated with individual differences in dispositional negativity.

Chapter 2: Methods

Participants

Demographic, imaging, and phenotypic data were extracted from the publicly available Nathan Kline Institute-Rockland Sample (NKI-RS) (http://fcon_1000.projects.nitrc.org/indi/enhanced/; Nooner et al., 2012) for 185 adults (18-40 years old). Exclusionary criteria included: positive drug urine screens (*n*=12), current psychiatric diagnosis at the time of the imaging session (*n*=14), incomplete MRI data (*n*=15), and incomplete phenotypic data (*n*=5). Using procedures described in more detail below, another 18 subjects were excluded due to motion artifact (*n*=8), susceptibility artifact (*n*=9), or distortion in the structural scan (*n*=1). The final sample is estimated to consist of about 130 subjects (59 males, mean age=25.32, standard deviation=6.12). **Table 1** presents the sample's demographic characteristics.

Quantifying Individual Differences in Dispositional Negativity

We used psychometrically sound measures of neuroticism (NEO Five Factor Inventory-3; NEO-FFI-3; McCrae & Costa, 2004) and its anxious facet (State and Trait Inventory; STAI; Speilberger et al., 1983) to quantify trait-like individual differences in dispositional negativity. The two scales were strongly correlated (*r*=0.79) and reliable (αs=0.84 and 0.92, respectively). Consistent with other work by our group (Shackman et al., *under review*), a composite measure of dispositional negativity was computed by taking the mean of the z-transformed scores (range of standardized scores: -1.80 to +2.64; α=0.88). **Supplementary Figure 1** presents the distribution of the z-transformed scores from the sample.

MRI Data Acquisition

MRI data were acquired using a Siemens Magnetom TrioTim 3T scanner and 32-channel coil. T1w anatomical images were acquired using a magnetization-prepared, rapid-acquisition, gradient-echo sequence (inversion time/repetition time/echo time/flip angle/field of view/matrix/slice thickness: 900 ms/1900 ms/2.52 ms/9°/250 mm^2/256 × 246/1 mm). Functional scans were obtained using a T_2*-weighted echo-planar image (EPI) sequence (multiband acceleration factor/repetition time/echo time/flip angle/number of excitations/field of view/matrix/in-plane resolution/slick thickness: 4/1400 ms/30 ms/65°/1/112 mm/112 × 112/2 mm × 2 mm; gap: 0 mm; 2mm slice thickness). All data were reconstructed on-line.

MRI Data Preprocessing

Unpublished pilot work by our group indicates that the quality of spatial normalization is enhanced by using a template and T1-weighted images that have been masked to remove extracerebral tissue (e.g., skull, meninges, cranial nerves; often termed 'skull-stripped'). However, this benefit is only realized when the masking quality is sufficiently high, as with images that have been manually masked by a well-trained neuroanatomist (e.g., Fox et al., 2015). To ensure high-quality masking, we used a multi-tool approach to automatically generate best-estimate masks for each T1-weighted image. For each T1-weighted image a total of six masks were generated. Five masks were generated using BET (Smith, 2002), BSE (Shattuck, Sandor-Leahy, Schaper, Rottenberg, & Leahy, 2001), 3dSkullstrip (Cox, 1996), ROBEX (Iglesias, Liu, Thompson, & Tu, 2011), and SPM unified segmentation (Ashburner & Friston, 2005), respectively. A sixth mask was generated by applying

the inverse transformation to the brain mask distributed with the MNI152 template[1]. A final mask was determined by consensus and required agreement across at least four of six tools. Using this best-estimate mask, each T1-weighted image was stripped of extracerebral tissue, inhomogeneity corrected using N4 (Tustison et al., 2014), and normalized to the 1-mm MNI152 template using the diffeomorphic approach implemented in SyN (Avants, Epstein, Grossman, & Gee, 2008; Avants et al., 2010; Avants, Tustison, Song, Cook, Klein, & Gee, 2011), the most accurate normalization tool (Klein et al., 2009).

The first 3 volumes of each EPI scan were removed and the remaining volumes were de-spiked and slice-time corrected using AFNI (Cox, 1996). Recent methodological work indicates that de-spiking is more effective than 'scrubbing' (Jo et al., 2013; Power, Schlaggar, & Petersen, 2015; Siegel et al., 2014) for attenuating motion-related artifacts in intrinsic functional connectivity. The spike- and motion-corrected images were co-registered to the masked, native-space T1w image using the boundary-based registration technique implemented in FSL (Greve & Fischl, 2009). Motion correction was performed using ANTS (Avants et al., 2009). To minimize spatial blurring, the transformation matrices for motion correction, co-registration, and spatial normalization to the MNI152 template was concatenated and applied to the EPI data in a single step. Normalized EPI data were resampled to 2-mm^3 voxels

[1]To mitigate risks to subject confidentiality, the publically released NKI-RS T1w images were masked by the database curators to remove skull and tissue in the region of the face ('de-faced'). The highly variable nature of the manual masking necessitated the development of specialized normalization techniques: (1) for each subject, the de-faced T1w image was spatially normalized to the 1-mm MNI152 template using the unified segmentation approach implemented in SPM12; (2) the 1-mm MNI152 template was de-faced to match the idiosyncratic de-facing of the T1w image; (3) the original T1w image was normalized to the individually de-faced 1-mm template using SyN; and (4) the inverse transformation was used to 'reverse-normalize' the brain mask distributed with the MNI152 template to native space.

using 5th–order splines.

To maximize spatial resolution, no additional spatial filters were applied (Stelzer, Lohmann, Mueller, Buschmann, & Turner, 2014; Turner & Gyer, 2014). EPI and T1w scans were visually inspected for quality assurance. The maximum value of the frame-to-frame displacement was calculated for each subject and transformed to *z*-scores in order to assess excessive motion. Subjects with a z-score greater than 1.96 were excluded (*n*=8). To assess signal dropout in the medial temporal lobe, mean signal ratios of regions of the amygdala relative to the caudate and putamen for each hemisphere for each subject were calculated and transformed to *z*-scores. Subjects with *z*-scores less than -2.50 were excluded (*n*=9). To attenuate physiological noise, white matter (WM) and cerebrospinal fluid (CSF) time-series were identified by thresholding the probabilistic segmented images provided with the MNI152 template. The 3 most prominent right eigenvectors of the data covariance matrix from each compartment, a fifth order Legendre polynomial, and motion estimates (6 parameters lagged by 0,1, and 2 volumes) were residualized from the EPI time series. Residualized data were bandpass filtered (0.009-0.10 Hz) using AFNI.

Seed Regions

The BST seed was determined by implementing a mask from previously published work (Theiss et al., 2016). The mask was originally manually prescribed on 10 T2-weighted (T2w) unique images by two observers using a manual segmentation protocol based on the atlas of Mai and colleagues (2007) and described in more detail in Theiss and colleagues (2016; **Figure 3a**).

Building on prior work by our group using similar methods (Birn et al.,

2014), the Ce was manually prescribed by a trained neuroanatomist (Dr. B. M. Nacewicz, Department of Psychiatry, University of Wisconsin—Madison; see also Nacewicz et al., 2014) based on the atlas of Mai and colleagues (2007) using the high-resolution (0.7-mm), multimodal (T1w/T2w) probabilistic template described in Tyszka and Pauli (2016; **Figure 3b**). Visual inspection indicated that, when combined with diffeomorphic normalization, this approach provides enhanced anatomical sensitivity and selectivity compared to the probabilistic CM amygdala seed distributed with the FSL software package (Amunts et al., 2005; **Supplementary Figure 2**). All seed regions were decimated to $2mm^3$.

Data Analysis Plan

We adopted a standard *a priori* seed-based approach to quantifying intrinsic functional connectivity (e.g., Biswal, Yetkin, Haughton, & Hyde, 1995; Fox et al., 2005). For each subject, we performed a voxelwise regression between the artifact-attenuated, average seed time-series and voxel times-series throughout the brain. Single-subject regression analyses was performed using the Cochrane-Orcutt procedure for estimating autoregressive error, which is more efficient and potentially less biased than ordinary least-squares (Stocker, 2007). In order to identify regions showing consistent functional connectivity with the BST or Ce seeds across subjects, we tested the intercept in regression models, equivalent to a single-sample *t* test ($p < .05$, whole-brain Šidák[2] corrected; ≥ 80 mm^3). A minimum conjunction (Boolean 'AND') was used to identify regions showing significant coupling with both seeds

[2] The Šidák correction ($\alpha_{Corrected} = 1 - (1 - \alpha_{Nominal})^{1/k}$, where k is the number of comparisons) is similar to but slightly more powerful than the more widely known Bonferroni procedure ($\alpha_{Corrected} = \alpha_{Nominal}/k$). Thus, for a family of k=100 tests, the Šidák procedure yields $\alpha_{Corrected} = 0.000513$, whereas the Bonferroni procedure yields $\alpha_{Corrected} = 0.0005$.

(Nichols et al., 2005) and a paired *t*-test was used to assess differential functional connectivity. For ease of interpretation[3], differential connectivity was only examined in the subset of 12,004 voxels where functional connectivity was significant for one or both seeds ($p < .05$, Šidák corrected for the 12,004 voxel region-of-interest; ≥ 80 mm^3).

A second series of whole-brain regression models were used to identify functional connections associated with individual differences in the composite measure of dispositional negativity. These analyses controlled for nuisance variation in mean-centered age and sex. Hypothesis testing employed statistical maps thresholded based on cluster extent ($p<.05$, whole-brain corrected; cluster-forming threshold: $p<.001$; Eklund, Nichols, & Knutsson, 2016; Friston, Worsley, Frackowiak, Mazziotta, & Evans, 1994). As an additional check on the integrity of the data and our approach, we confirmed our ability to identify the default mode network (**Supplementary Figure 3**). As a supplement to hypothesis testing, we also assessed, on an exploratory basis, the intrinsic functional connectivity of the more widely used Jülich CMA seed (**Supplementary Figure 4**).

[3] This circumvents the need to interpret significant differences (e.g., BST > Ce) in regions where neither seed shows significant levels of functional connectivity.

Chapter 3: Results

Subcortical Results

As shown in **Figure 4**, results revealed robust coupling between the two poles of the central extended amygdala. Analyses seeded at either pole were associated with significant coupling with neighboring voxels and with voxels at the opposite pole (**Tables 2-4**). Thus, the BST showed significant connectivity with adjacent regions of the basal forebrain and basal ganglia as well as distal voxels located in the region of the Ce. Conversely, the Ce showed significant coupling with adjacent regions of the dorsal amygdala and with distal voxels located in the region of the BST. Consistent with invasive anatomical tracing studies (Oler et al., 2016), the BST and Ce also showed robust coupling with intermediate voxels located in the sublenticular extended amygdala, the ribbon of subcortical gray matter ('substantia innominata') encompassing the ventral amygdalofugal pathway (**Figure 5**). In addition, both seeds showed significant functional connectivity with the anterior hippocampus (**Figure 4; Tables 2-4**).

Relative to the Ce, the BST showed significantly stronger coupling with the basal ganglia, including the caudate, putamen, and nucleus accumbens, as well as the thalamus and periaqueductal gray (**Figure 4** and **Table 5**). The only subcortical regions showing stronger connectivity with the Ce were neighboring regions of the amygdala, including voxels located in the probable region of the amygdalohippocampal area and basolateral, basomedial, cortical, and medial nuclei.

Cortical Results

Cortically, the BST and Ce both showed significant coupling with regions of the ventral visual processing stream, including the superior temporal sulcus and fusiform cortex (**Figure 4** and **Tables 2-4**). As shown in **Figures 4** and **7**, both seeds also exhibited significant functional connectivity with the posterior cingulate/precuneus; posterior insula, focused on the dorsal region of the long gyri; posterior midcingulate cortex, and ventromedial prefrontal cortex (vmPFC). Compared to the Ce, the BST shows significantly stronger coupling with more rostral regions of the cingulate, including the anterior midcingulate and pregenual anterior cingulate cortices (**Table 5**). The BST also shows significantly stronger connectivity with the vmPFC. As shown in **Figure 7**, the vmPFC cluster extended from area 10r/m to the pregenual anterior cingulate cortex and included parts of the inferior frontopolar and rostral gyri.

Individual Differences in Dispositional Negativity

Contrary to expectation, BST and Ce functional connectivity was not significantly associated with individual differences in either the composite measure of dispositional negativity or its constituents, neuroticism and trait anxiety.

Chapter 4: Discussion

In the current study, we delineated the intrinsic functional connectivity of the central extended amygdala in a community-dwelling sample of 130 healthy adults and assessed the relationship between connectivity patterns and self-reported dispositional negativity. We observed patterns of intrinsic functional connectivity maps broadly consistent with prior work in animals and humans and novel findings demonstrating reciprocal intrinsic functional connectivity between the Ce and BST.

The Central Extended Amygdala as a Functional Unit

Consistent with invasive tracing studies in nonhuman primates (Oler et al., 2016), we observed robust reciprocal coupling between the BST and Ce. Both regions also showed significant connectivity with voxels located in the SLEA, which can be seen connecting the BST seeds through the nucleus accumbens and the distal amygdala voxels in the region of the Ce via the ventroamygdalofugal path. These observations align with recent work in humans that exploited the enhanced spatial resolution (1.3 mm^3 native resolution and a 2.6-mm smoothing kernel) afforded by ultra-high field strength (7 Tesla) MRI to demonstrate significant functional connectivity between the BST and dorsal amygdala, including the probable location of the Ce (Torrisi et al., 2015).

Some investigators have suggested that the Ce and BST are better conceptualized as "differentiated" striatopallidum embedded in a larger stratopallidal projection system rather than a unique functional unit (Swanson, 2003). Taken

together with work from colleagues (Birn et al., 2014, Oler et al., 2012; 2016; Torrisi et al., 2015), our findings present additional evidence that functional activations, as indexed by BOLD signal, are highly coordinated between the BST and Ce and their unique connectivity sets them apart from the striatum and pallidum. Additionally, our findings underscore the potential importance of SLEA as a communication center for extended amygdala information processing.

The Central Extended Amygdala and Responses to Threat

We observed more robust BST intrinsic functional connectivity with the PAG relative to the Ce, which aligns with previous human BST connectivity patterns observed in Torrisi and colleagues (2015) and Avery and colleagues (2014) as well as findings from anatomical studies in rodents and monkeys (Aggleton & Mishkin, 1984; Dong & Swanson, 2004). The PAG is involved in emotion, pain, and physiological and behavioral defensive responses (LeDoux, Iwata, Cicchetti, & Reis, 1988; Bandler, Price, & Keay, 2000; Nashold, Wilson, & Slaughter, 1969; Satpute et al., 2013) and thus, our findings are consistent with the idea that the BST plays a role in initiating defensive responses to environmental threat. Additionally, both the Ce and BST showed coupling to regions of the striatum, hippocampus –a subcortical structure critical for contextual conditioning (Maren, Phan, & Liberzon, 2013), and regions in the ventral visual processing stream, including the superior temporal sulcus and fusiform cortex – structures that form the core system for social perception and decoding social intentions and interactions (Dziobek, Bahnemann, Convit, & Heekeren, 2010; Tyler et al., 2013). Functional connectivity with these structures lends evidence for the extended amygdala's potential role in influencing neural

networks that support operant, sensory, and cognitive responses to stimuli in the environment (Shackman et al., 2016b).

Notably, the BST, relative to the Ce, exhibited stronger functional connectivity with the ventral striatum and other regions involved in the orchestration of motivated behavioral responses. These regions consisted of clusters corresponding to midcingulate and pregenual anterior cingulate cortices as well as the caudate, putamen, and nucleus accumbens. In rats, the BST, compared to the Ce, has been shown to receive more afferent inputs from regions associated with motor function including the nucleus accumbens (Bienkowski & Rinaman, 2012). Recent findings in humans have demonstrated that the caudate nucleus and the BST are strongly functionally connected (Avery et al., 2014; Torrisi et al., 2015) and that fiber paths connect the BST to the medial prefrontal cortex via the head of the caudate (Krüger, Shiozawa, Kreifelts, Scheffler, & Ethofer, 2015). Investigators have posited that one way compulsive and drug seeking behaviors emerge and are reinforced during anxious states could potentially be through the interaction between the BST and ventral striatum (Koob & Volkow, 2010; Berridge, Robinson, & Aldridge, 2009).

While our findings of Ce functional connectivity with midcingulate cortex is consistent with investigations in nonhuman primates (Birn et al., 2014) and humans (Oler et al., 2012), the robust coupling that we detected between the BST, relative to the Ce, and regions of the anterior midcingulate and pregenual anterior cingulate is novel. The anterior midcingulate is thought to play a role in negative affect, pain, and cognitive control and to play a crucial role in regulating behavior in the face of uncertainty about actions and their potentially aversive outcomes (Shackman et al.,

2011; Cavanagh & Shackman, 2015). The pregenual anterior cingulate has been implicated in the generation of affect and in predicting treatment response in anxiety (Whalen et al., 2008) and depression (Mayberg, 1997; Pizzagalli, 2011).

The BST also exhibited stronger coupling with the vmPFC relative to the Ce, and these findings mirror previous work examining BST intrinsic functional connectivity in humans (Avery et al., 2014; Motzkin et al., 2015; Torrisi et al., 2015) and complement mechanistic work demonstrating that damage to the vmPFC is associated with reductions in BST metabolism (Fox et al., 2010), BST perfusion (Motzkin et al., 2015), and anxiety-related behaviors, such as threat-elicited freezing (Fox et al., 2010). For example, Motzkin and colleagues (2015) demonstrated a selective reduction in BST perfusion in a sample of patients with vmPFC damage. In an independent sample of healthy young adults, they demonstrated significant functional connectivity between the two regions. On this basis, the authors hypothesized that the vmPFC typically plays a role in promoting BST activity, which in turn, serves to promote the expression of fear and anxiety in the presence of potential threat (Walker et al., 2003). Our findings further support this putative interaction and highlight the need to understand how vmPFC-BST circuitry could update models of mood, anxiety, and addiction disorders (as previous models largely focus on vmPFC-amygdala inhibition; e.g., Quirk and Gehlert, 2003).

Given the preponderance of evidence supporting the importance of the central extended amygdala to facets of DN, including processing and goal-directed behavior in the face of threat, the lack of observed association between intrinsic functional connectivity and DN is surprising. Although our study provides substantially greater

power than many prior studies of amygdalar resting-state functional connectivity, it remains possible that the magnitude of the association between functional connectivity and individual differences in DN is too small to reliably detect with a sample of the present size. Another possibility is that self-report measures of DN are insufficiently sensitive. Other studies that have reported significant associations between facets of DN and amygdala resting-state functional connectivity have relied on observer-defined behavioral measures (Roy et al., 2014; Birn et al., 2014 - monkeys) or clinician-defined psychiatric diagnoses (Birn et al., 2014 - humans; Roy et al., 2013; for a meta-analysis see Marusak et al., 2016)

Limitations and Future Directions

There were several limitations to this study. First, resting state functional connectivity cannot address the directionality of connectivity between structures and thus, flow of information and order of processes cannot be determined. Second, functional connectivity cannot address whether the source of connectivity is via monosynaptic or polysynaptic pathways, which further reduces our ability to understand the flow of emotion-relevant information across the the extended amygdala circuit. For example, the connections between the Ce and BST may be due to direct monosynaptic connections (e.g., via the ventral amygdalofugal pathway; **Figure 2**) or driven by shared afferent inputs from another region. Third, the data in this study only reflect resting-state functional connectivity; differing connectivity patterns and associations with individual differences may emerge in response to threat-related cues. Fourth, other regions of amygdala, such as the basolateral complex, and other regions of the central extended amygdala (including the nucleus

accumbens shell and the stria terminalis) likely contribute to stress-sensitive neural networks. In order to continue to elucidate the neural circuitry involved in the expression of DN and eventual relevance to adverse outcomes such as psychopathology, future work will need to employ larger samples, emotion induction paradigms, and increasingly anatomically precise regions of interest for smaller, functionally distinct territories.

Conclusions

Our findings extend previous work on the intrinsic functional connectivity of the two main poles of the central extended amygdala, the BST and Ce. The cortical and subcortical regions identified by the functional mapping of the BST and Ce network include areas that are particularly important in orchestrating both behavioral and physiological responses to integrated information about stress and threat. These results emphasize the need to examine small but important structures in psychiatric neuroimaging research and update existing neurobiological models of DN, anxiety, depression, and addiction.

Tables

Table 1.

Sample demographics.

Demographic variable	
Age	25.32 (6.12)
Male/Female	59/71
Race, *n* (%)	
White, European-American	71 (54.6%)
African-American	38 (29.2%)
Asian	13 (10%)
Other	8 (21.8%)
Ethnicity, *n* (%)	
Hispanic/Latino descent	18 (13.85%)

Table 2. *Regions showing significant functional connectivity with the BST**

MNI x	***MNI y***	***MNI z***	***t***	**Volume (mm^3)**	**Hemisphere**	**Region(s)/*Subregions***
11	45	1	7.65	176	B	Cingulate sulcus, pregenual
-21	41	29	8.55	352	L	Superior frontal sulcus, anterior
-25	33	49	10.03	896	L	Superior frontal sulcus, anterior
27	32	35	8.75	888	B	Superior frontal sulcus, anterior
-42	23	-5	7.86	272	L	Orbitofrontal cortex, basal operculum
-5	3	0	21.04	49,072	B	Midline
-6	4	-1	21.04	9,128	B	*Basal forebrain: Caudate, Putamen, Globus pallidus, Nucleus accumbens, Piriform cortex, Sublenticular extended amygdala (ventral amygdalofugal pathway), Dorsal amygdala (Central and Medial nuclei), Anterior hippocampus, Thalamus, Brainstem*
-6	-43	5	12.96	7,648	B	*Posterior cingulate/Precuneus*
1	19	37	11.70	3,072	L	*Cingulate: Cingulate sulcus, midcingulate; Cingulate sulcus, posterior; Juxtapositional lobule*
11	18	33	10.27	480	R	*Cingulate: Cingulate sulcus, pregenual; Cingulate sulcus, midcingulate*
1	53	-5	9.67	328	B	*Ventromedial prefrontal cortex: OP10r/m**; Inferior frontopolar gyrus; Rostral gyrus; Anterior cingulate cortex, pregenual*
-3	-25	-3	9.48	80	L	*Periaqueductal gray, dorsolateral*
-53	2	-1	7.97	136	L	Superior temporal gyrus, planum polare
-39	1	59	7.12	136	L	Precentral sulcus
1	-13	-23	8.81	88	R	Cerebellum
-37	-15	17	10.79	1,648	L	Posterior insula: Central operculum, parietal operculum, posterior insula (dorsal portion of the long gyri), Heschl's gyrus
53	-16	5	9.57	2,224	R	Posterior insula: Central operculum, parietal operculum, posterior insula (dorsal portion of the long gyri), Heschl's gyrus
31	-17	3	7.43	184	R	Putamen

13	-17	39	8.01	160	B	Cingulate sulcus, posterior
-27	-19	5	7.91	112	L	Putamen
7	-21	-1	10.85	152	R	Thalamus
69	-22	-3	8.19	544	R	Superior temporal sulcus
-20	-29	57	11.70	3,144	L	Central sulcus
21	-29	57	13.12	3,024	R	Central sulcus
26	-37	57	8.98	360	B	Postcentral sulcus
-19	-37	65	8.04	272	L	Postcentral gyrus
57	-57	21	7.53	176	R	Angular gyrus
54	-62	31	7.04	176	R	Lateral occipital cortex
-9	-69	5	8.29	256	L	Calcarine sulcus
31	-72	-37	8.41	344	B	Cerebellum
-31	-80	-37	8.17	504	L	Cerebellum
-7	-81	1	7.94	384	L	Calcarine sulcus
-35	-83	-19	7.03	96	L	Lateral occipital cortex/Fusiform, occipital
25	-85	-19	8.08	328	R	Fusiform, occipital
15	-93	1	7.90	80	R	Occipital pole

* Whole-brain regression analysis ($p<.05$, whole-brain Šidák corrected, $k\geq80$ mm^3). ** Area 10r/m as describe by Ongur and colleagues (2003). Abbreviations—B**,** Bilateral; BST, bed nucleus of the stria terminalis; L, left hemisphere; R, right hemisphere.

Table 3. *Regions showing significant functional connectivity with the Ce**

MNI x	***MNI y***	***MNI z***	***t***	**Volume(mm^3)**	**Hemisphere**	**Region(s)/*Subregions***
1	59	19	8.29	504	B	Dorsomedial prefrontal cortex: BA10
1	53	-13	8.70	600	B	Ventromedial prefrontal cortex: OP10r/m**; Inferior frontopolar gyrus; Rostral gyrus
8	39	-15	7.27	112	R	Ventromedial prefrontal cortex: Inferior frontopolar gyrus, Straight gyrus
34	37	-13	7.15	96	R	Orbitofrontal cortex: OP11**, Anterior orbital gyrus
-19	37	43	7.92	392	L	Superior frontal sulcus, anterior
39	9	-15	7.84	176	R	Anterior insula: Transverse insular gyrus
9	3	3	10.11	424	R	Basal forebrain: Caudate, Bed nucleus of the stria terminalis
-5	1	1	10.56	376	L	Basal forebrain: Caudate, Bed nucleus of the stria terminalis
57	-5	23	12.64	12,736	B	Central cortex
57	-5	23	12.64	3,024	R	*Central sulcus*
-3	-22	45	10.87	1,096	B	*Cingulate sulcus, posterior; Cingulate sulcus, midcingulate*
-1	-31	57	8.44	160	B	*Precentral gyrus*
-52	-7	25	11.53	6,912	L	Central sulcus
23	-9	-13	22.02	2,696	R	Basal forebrain: Piriform cortex, Sublenticular extended amygdala (ventral amygdalofugal pathway), Amygdala (Amygdalohippocampal area, Basolateral, Basomedial, Cortical, Lateral, and Medial), Anterior hippocampus, Brainstem
-19	-11	-13	20.91	2,720	L	Basal forebrain: Putamen, Piriform cortex, Sublenticular extended amygdala (ventral amygdalofugal pathway), Amygdala (Amygdalohippocampal area, Basolateral, Basomedial, Cortical, Lateral, and Medial), Anterior hippocampus, Brainstem
51	-12	-13	10.60	4,904	R	Temporal lobe: Superior temporal gyrus, Planum polare; Parietal operculum; Superior temporal sulcus;
-37	-15	17	10.73	6,400	L	Posterior insula: Central operculum, parietal operculum, posterior insula (dorsal portion of the long gyri), Planum temporale, Heschl's gyrus, Superior temporal sulcus
39	-15	17	10.89	1,096	R	Posterior insula: Central operculum, parietal operculum, posterior insula (dorsal portion of the

						long gyri)
53	-23	45	6.38	80	R	Postcentral sulcus
53	-27	57	6.73	104	R	Postcentral gyrus
25	-37	59	8.30	592	R	Postcentral sulcus
-44	-50	-17	8.10	192	L	Temporal lobe: Inferior temporal gyrus, temporooccipital; Fusiform, temporooccipital
37	-52	-21	7.99	208	R	Temporal lobe: Inferior temporal gyrus, temporooccipital; Fusiform, temporooccipital
-1	-53	17	13.43	7,632	B	Posterior cingulate/Precuneus
57	-63	11	9.33	2,272	R	Lateral occipital cortex
29	-83	-19	6.39	88	R	Fusiform, occipital

* Whole-brain regression analysis (p<.05, whole-brain Šidák corrected, k≥80 mm^3). Sub-regions are reported in italics. ** Areas 10r/m and 11 as describe by Ongur and colleagues (2003). Abbreviations—B, bilateral; Ce, central nucleus of the amydala; L, left hemisphere; R, right hemisphere.

Table 4. *Regions showing significant functional connectivity with both the BST and Ce**

MNI x	*MNI y*	*MNI z*	*t*	Volume (mm^3)	Hemisphere	Region(s)
1	61	21	n/a	48	R	Dorsomedial prefrontal cortex: BA10
3	59	17	n/a	16	R	Dorsomedial prefrontal cortex: BA10
1	57	13	n/a	24	R	Dorsomedial prefrontal cortex: BA10
1	53	19	n/a	80	R	Dorsomedial prefrontal cortex: BA10
-1	49	27	n/a	24	L	Dorsomedial prefrontal cortex: BA10
1	39	-15	n/a	296	R	Ventromedial prefrontal cortex: OP10r/m **; Inferior frontopolar gyrus; Rostral gyrus
-21	27	37	n/a	304	L	Superior frontal sulcus, anterior
55	7	-3	n/a	8	R	Temporal pole
63	7	-1	n/a	664	R	Planum temporale
9	5	-1	n/a	384	R	Basal forebrain: Caudate, Bed nucleus of the stria terminalis
-9	5	35	n/a	3,448	L	Cingulate: Cingulate sulcus, posterior midcingulate; Cingulate sulcus, posterior
-5	3	-1	n/a	312	L	Basal forebrain: Caudate, Bed nucleus of the stria terminalis
5	1	-3	n/a	8	R	Bed nucleus of the stria terminalis
-53	1	-1	n/a	40	L	Planum polare
53	1	-1	n/a	24	R	Planum polare
-1	1	47	n/a	8	L	Juxtapositional lobule
-17	-3	-15	n/a	376	L	Dorsal amygdala: Amygdalohippocampal area, Central, Cortical, Medial
63	-3	17	n/a	2,640	R	Central sulcus
61	-5	-13	n/a	392	R	Superior temporal sulcus
29	-11	-23	n/a	976	R	Hippocampus
-41	-15	31	n/a	2,648	L	Central sulcus
5	-15	73	n/a	8	R	Precentral gyrus

63	-17	-7	n/a	8	R	Superior temporal sulcus
-53	-17	9	n/a	8	L	Heschl's gyrus
-21	-19	-17	n/a	616	L	Hippocampus/Dorsal amygdala: Basolateral, Basomedial, Central, Medial
-57	-19	9	n/a	152	L	Planum temporale
13	-19	39	n/a	40	R	Cingulate sulcus, posterior
3	-19	67	n/a	16	R	Precentral gyrus
-47	-25	3	n/a	880	L	Planum temporale
47	-25	7	n/a	728	R	Planum temporale
-25	-31	67	n/a	96	L	Postcentral gyrus
3	-33	49	n/a	16	R	Posterior cingulate
27	-37	55	n/a	232	R	Postcentral sulcus
-21	-39	63	n/a	128	L	Postcentral gyrus
3	-39	63	n/a	8	R	Postcentral gyrus
11	-53	1	n/a	6,792	R	Posterior cingulate/Precuneus
55	-57	19	n/a	136	R	Angular gyrus
45	-59	29	n/a	8	R	Lateral occipital cortex
31	-85	-19	n/a	88	R	Occipital fusiform

* Minimum conjunction (Boolean 'AND') analysis ($p<.05$, whole-brain Šidák corrected, $k\geq80$ mm^3). ** Area 10r/m as describe by Ongur and colleagues (2003). Abbreviations—B, bilateral; BST, bed nucleus of the stria terminalis; Ce, central nucleus of the amydala; L, left hemisphere; R, right hemisphere.

Table 5. *Regions showing significant differential functional connectivity between BST and Ce**

	MNI x	*MNI y*	*MNI z*	*t*	Volume (mm^3)	Hemisphere	Region(s)
BST>Ce							
	-25	55	31	6.80	80	L	Frontal pole: BA9/BA10
	2	45	-1	8.43	344	B	Ventromedial prefrontal cortex: OP10r/m**; Inferior frontopolar gyrus; Rostral gyrus; Anterior cingulate, pregenual
	21	41	31	7.12	96	R	Superior frontal sulcus, anterior
	-25	41	35	5.69	112	L	Superior frontal sulcus, anterior
	11	37	-3	7.11	96	R	Cingulate: Cingulate sulcus, pregenual
	7	36	25	9.94	3,504	B	Cingulate: Cingulate sulcus, pregenual; Cingulate sulcus, anterior midcingulate
	49	23	-9	7.53	80	R	Orbitofrontal cortex: OP47, Basal operculum
	6	5	-2	17.15	10,472	B	Basal forebrain: Caudate, Putamen, Globus pallidus, Nucleus accumbens, Sublenticular extended amygdala (ventral amygdalofugal pathway), Thalamus
	3	-11	35	6.73	128	R	Posterior cingulate
	-1	-17	-21	7.06	80	L	Brainstem ventral to the interpeduncular cistern
	-3	-23	-1	7.34	112	L	Periaqueductal gray, dorsolateral
	5	-24	-3	8.38	136	R	Periaqueductal gray, dorsolateral
	3	-27	25	10.17	968	B	Posterior cingulate
	4	-35	47	8.45	800	B	Posterior cingulate
	13	-47	31	5.94	104	R	Posterior cingulate
	-7	-69	33	8.82	288	L	Precuneus
	1	-75	43	6.89	232	B	Precuneus
	-8	-81	3	6.86	216	L	Calcarine sulcus
	9	-87	1	7.59	488	R	Calcarine sulcus

Ce>BST							
	25	-9	-15	-14.31	536	R	Anterior hippocampus and Amygdala: Amygdalohippocampal area, Basolateral, Basomedial, Cortical, Medial
	-21	-10	-15	-11.19	504	L	Amygdala: Amygdalohippocampal area, Basolateral, Basomedial, Cortical, Medial

* Paired t-test for the subset of 12,004 voxels (2-mm^3) showing significant functional connectivity with the BST, Ce, or both seeds (p<.05, Šidák corrected for the extent of the 12,004-voxel mask). ** Area 10r/m as describe by Ongur and colleagues (2003). Abbreviations—B, bilateral; BST, bed nucleus of the stria terminalis; Ce, central nucleus of the amydala; L, left hemisphere; R, right hemisphere.

Figures

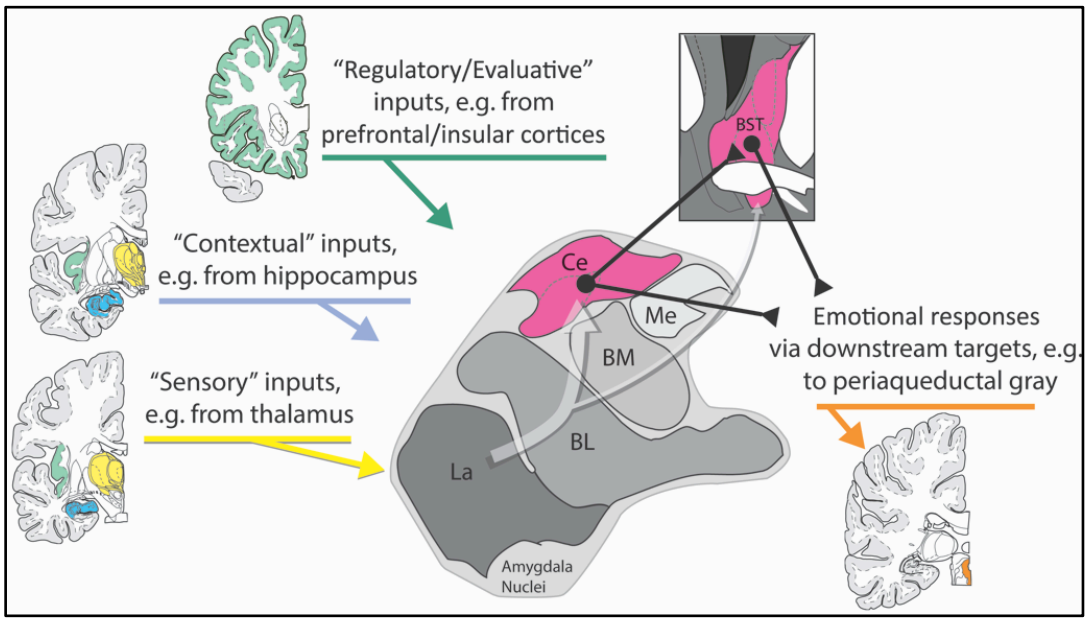

Figure 1. Primate central extended amygdala. Simplified schematic of key central extended amygdala inputs and outputs in humans and other primates. The central extended amygdala (*magenta*) encompasses the central nucleus of the amygdala (Ce) and the bed nucleus of the stria terminalis (BST), which wraps around the anterior commissure. As shown by the translucent white arrow at the center of the figure, much of the sensory (*yellow*), contextual (*blue*), and regulatory (*green*) inputs to the central extended amygdala are indirect (i.e., polysynaptic), and often first pass through adjacent amygdala nuclei before arriving at the BST or Ce. Among primates, both regions are poised to orchestrate momentary states of fear and anxiety via projections to downstream effector regions (*orange*). Portions of this figure were adapted from the atlas of Mai et al. (2007). See also Yilmazer-Hanke (2012). Abbreviations—BL, basolateral nucleus of the amygdala; BM, basomedial nucleus of

the amygdala; BST, bed nucleus of the stria terminalis; Ce, central nucleus of the amygdala; La, lateral nucleus of the amygdala; Me, medial nucleus of the amygdala.

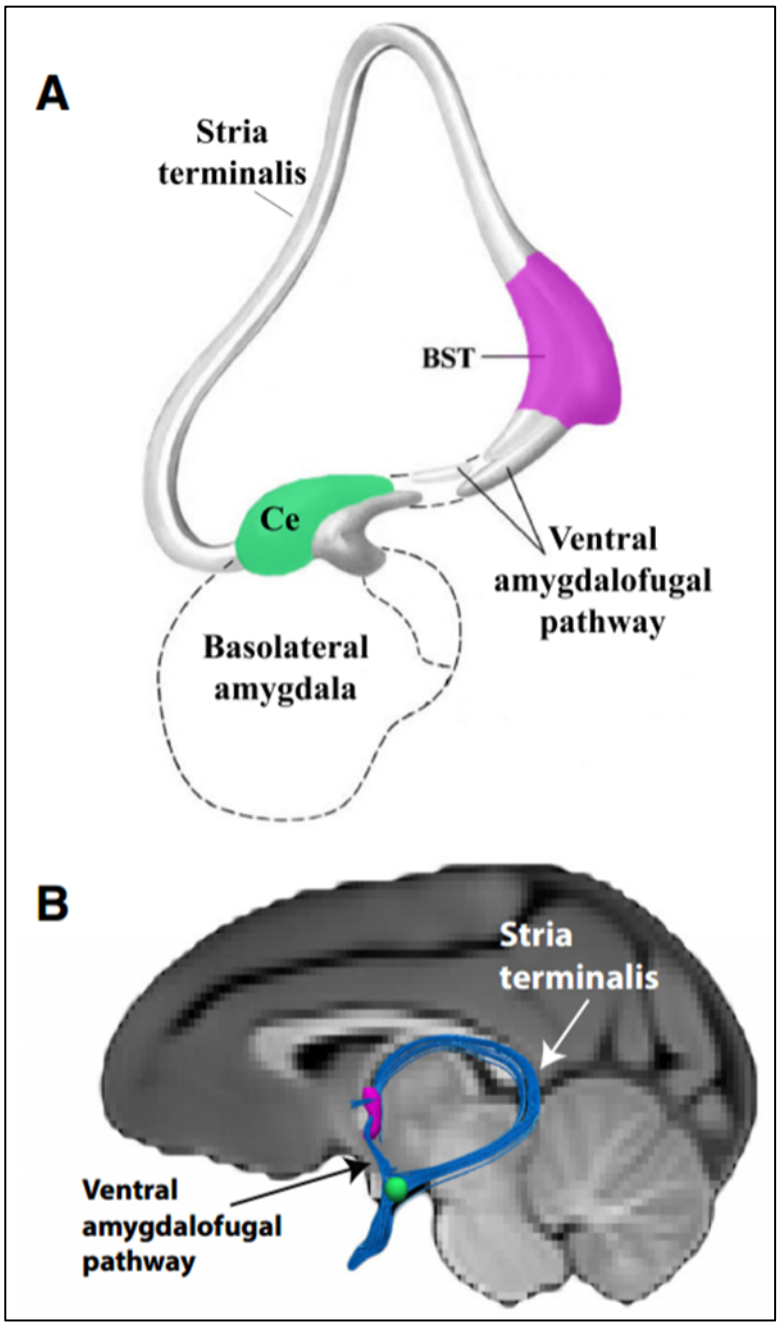

Figure 2. Structural connections of the central extended amygdala. In humans and other primates, the BST (*green*) and Ce (*magenta*) are structurally connected via two major fiber bundles, the ventral amygdalofugal pathway and the stria terminalis (Johnston, 1923; Nauta, 1961; Yilmazer-Hanke, 2012). From the Ce, the ventral

amygdalofugal pathway courses forward and medially, passing through the sublenticular extended amygdala (SLEA), a bridge of neurons harbored within the substantia innominata. Recent tracing studies suggest that the SLEA represents a key structural hub for communications between the BST and Ce (Ce ↔ SLEA ↔ BST; Oler et al., 2016). The stria terminalis, which arches dorsally over the thalamus, provides a second, less direct connection between the two poles of the central extended amygdala. **A.** Schematic depiction of the major structural pathways linking the BST to the Ce. **B.** Deterministic tractography (*dark blue*) of the central extended amygdala in the monkey. This figure is reproduced from Oler et al. (2016). Panel A includes artwork originally adapted from Heimer et al. (1999). Abbreviations—BST, bed nucleus of the stria terminalis; Ce, central nucleus of the amygdala.

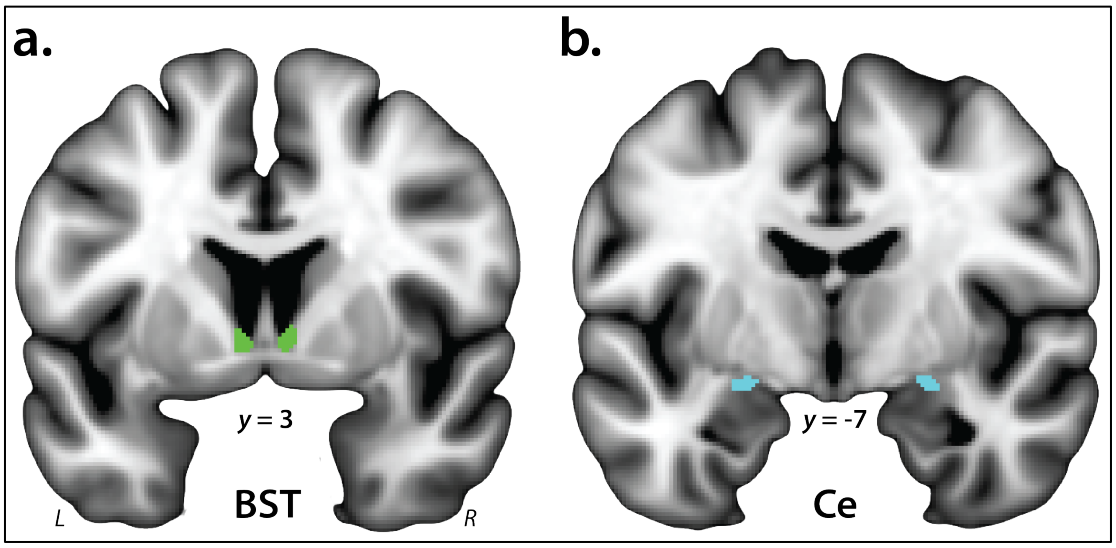

Figure 3. Bed Nucleus of the Stria Terminalis (BST) and Central Nucleus of the Amygdala (Ce) Seeds. The derivation of the probabilistic BST seed (*green*) is described in more detail in Theiss and colleagues (2016) and was thresholded at 25%. The seed mostly encompasses the supra-commissural BST, given the difficulty of reliably discriminating the borders of regions below the anterior commissure on the basis of T1-weighted MRI (Kruger, Shiozawa, Kreifelts, Scheffler, & Ethofer, 2015). Building on prior work by our group (Birn et al., 2014; Oler et al., 2012; 2016), the Ce seed (*cyan*) was manually prescribed by a trained anatomist (B.M. Nacewicz) based on the atlas of Mai and colleagues (Mai et al., 2007) and using a high-resolution (0.7-mm), multi-modal (T1w/T2w) probabilistic MRI template (Tyszka & Pauli, 2016) . For illustrative purposes, 1-mm seeds are shown. Analyses employed seeds decimated to the 2-mm resolution of the EPI data. Single-subject structural data were visually inspected to ensure that the seeds were correctly aligned to the spatially normalized anatomical (T1w) images. Abbreviations—L, left hemisphere; R, right hemisphere.

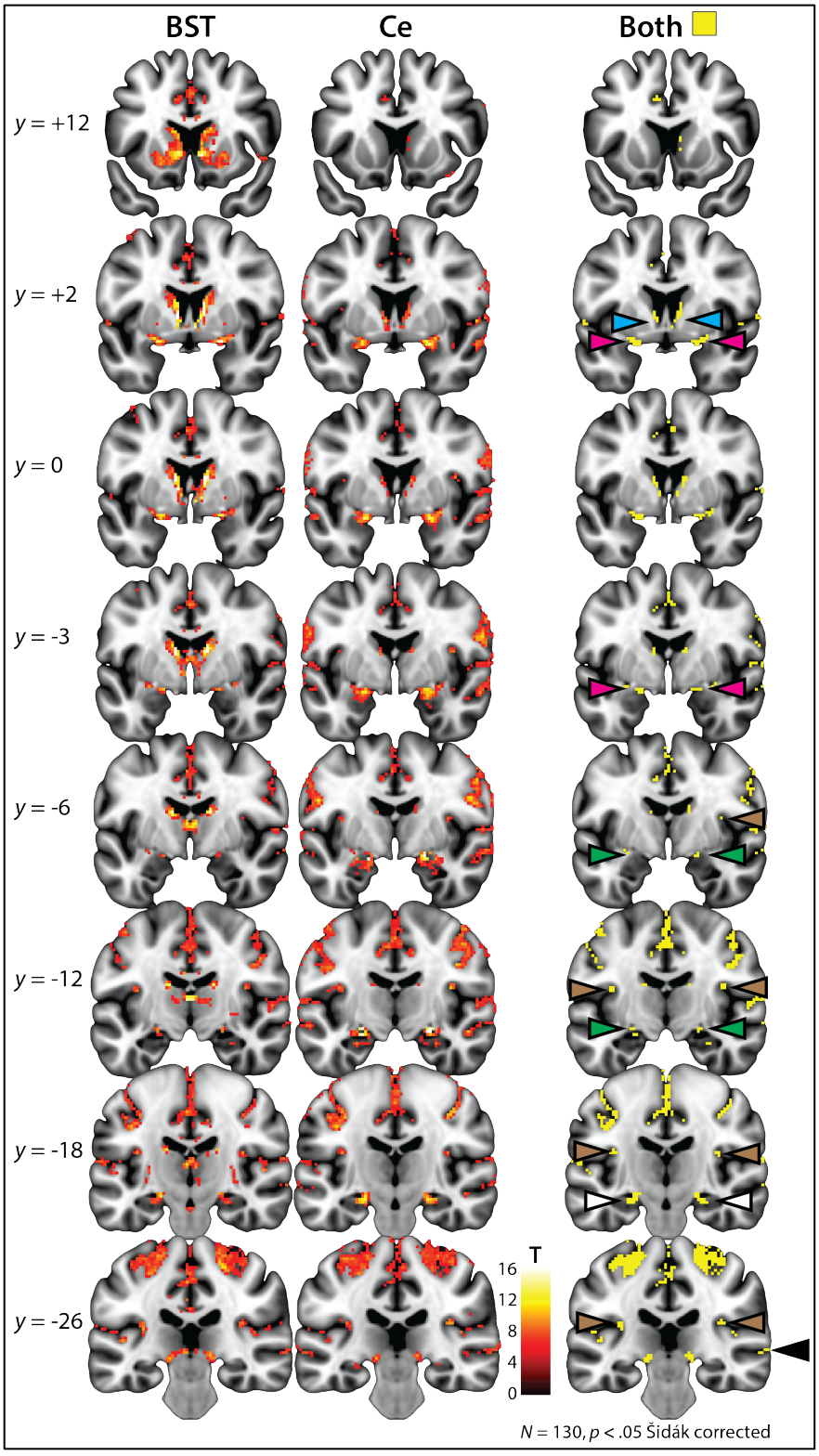

Figure 4. Basal Regions Showing Significant Functional Connectivity with the Bed Nucleus of the Stria Terminalis (BST) and Central Nucleus of the Amygdala (Ce).

Left and center columns depict the results of whole-brain regression analyses for the

BST and Ce seed regions, respectively, conservatively thresholded at $p<.05$ whole-brain Šidák corrected. The right column depicts the intersection (Boolean 'AND') of the two thresholded maps (Nichols, Brett, Andersson, Wager, & Poline, 2005). Analyses seeded in either pole of the central extended amygdala revealed significant coupling with neighboring voxels as well as voxels at the opposite pole. Thus, the BST seed showed significant functional connectivity with neighboring basal forebrain voxels (*cyan* arrowheads) and with distal amygdala voxels in the region of the Ce (*green* arrowheads). Similarly, the Ce seed showed significant coupling with dorsal amygdala voxels and with distal voxels in the region of the BST. Analyses also demonstrated that the BST and Ce exhibit robust functional connectivity with intermediate voxels located along the path of the ventral amygdalofugal patheway in the sublenticular extended amygdala (*magenta* arrowheads). Finally, both regions showed significant coupling with the anterior hippocampus (*white* arrowheads), posterior insula (*brown* arrowheads), and superior temporal sulcus (*black* arrowheads). Note: Results are depicted here and reported in the accompanying tables for clusters of at least 80 mm^3. Abbreviations—BST, bed nucleus of the stria terminalis; Ce, central nucleus of the amygdala; L, left hemisphere; R, right hemisphere.

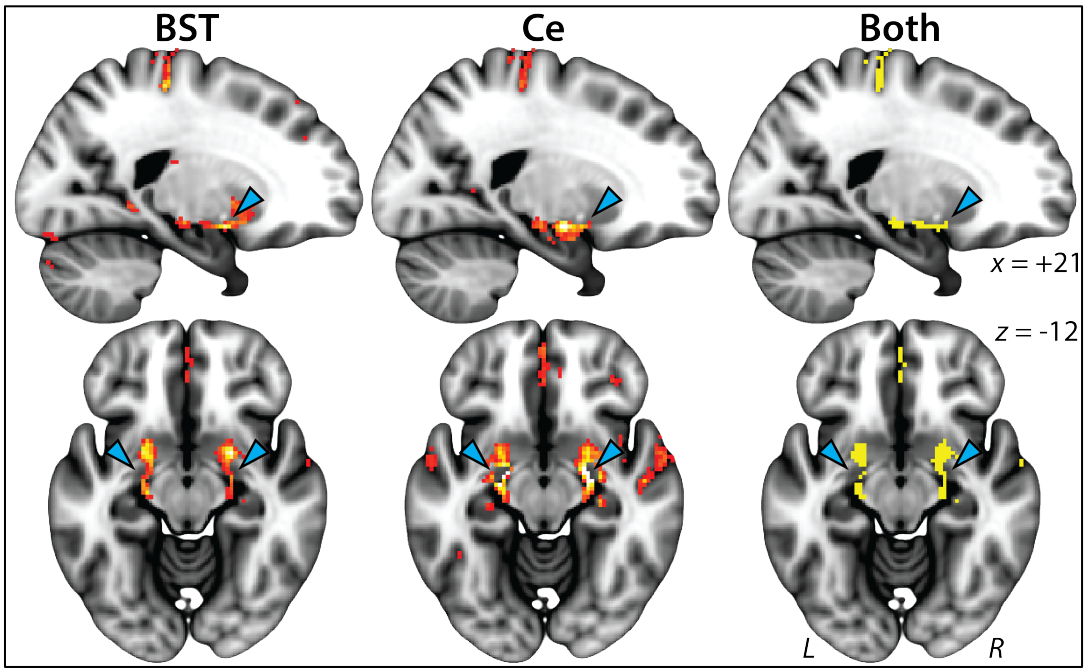

Figure 5. The Bed Nucleus of the Stria Terminalis (BST) and Central Nucleus of the Amygdala (Ce) are Functionally Linked via the Sublenticular Extended Amygdala (SLEA). Clusters in the region of the SLEA (*cyan* arrowheads). Conventions are similar to Figure 4. Abbreviations—BST, bed nucleus of the stria terminalis; Ce, central nucleus of the amygdala; L, left hemisphere; R, right hemisphere.

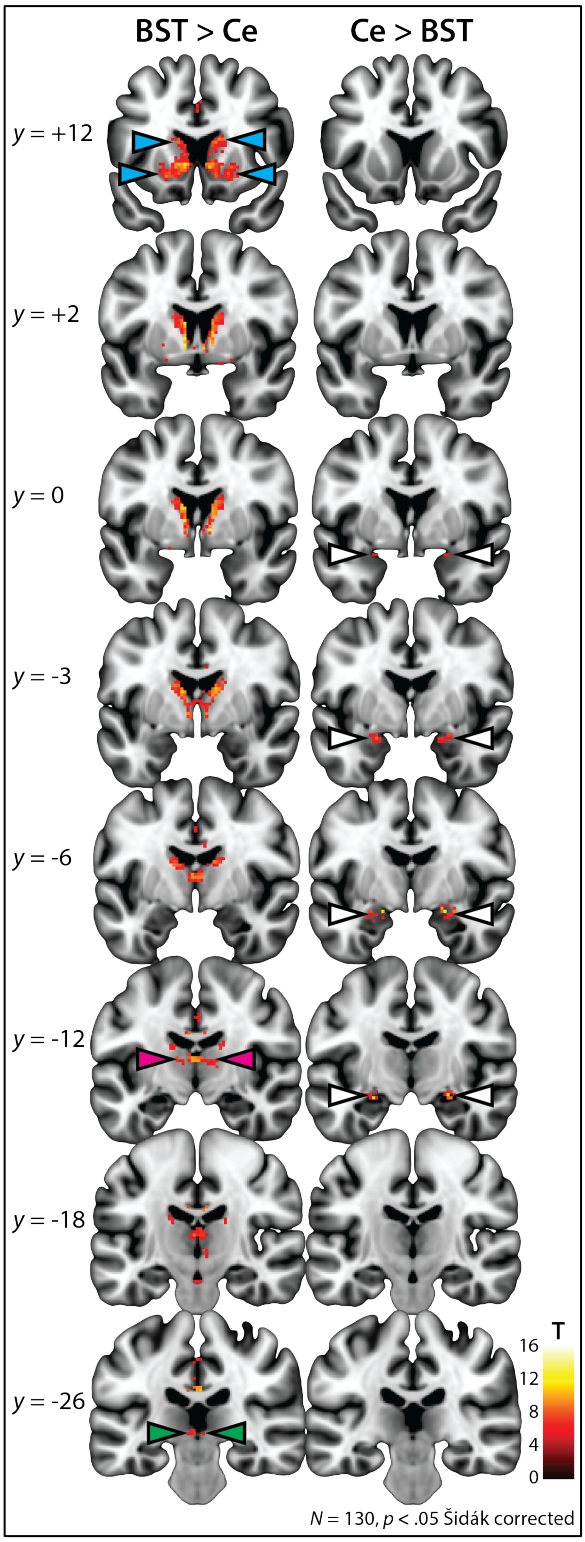

Figure 6. Basal Regions Showing Differential Functional Connectivity with the Bed Nucleus of the Stria Terminalis (BST) and Central Nucleus of the Amygdala (Ce).

Results of a paired *t*-test comparing the intrinsic functional connectivity of the BST

and Ce. The left and right columns depict regions showing significantly stronger coupling with the BST and Ce, respectively. For ease of interpretation, differences were only examined in the subset of 12,004 voxels (2-mm^3) where functional connectivity was significant for the BST, Ce, or both seeds (shown in Figures 4-5). Paralleling our other analyses, results were thresholded at $p<.05$ Šidák corrected for the extent of the 12,004-voxel mask. Results revealed significantly stronger coupling between the BST and the basal ganglia, including the caudate, putamen, and nucleus accumbens (*cyan* arrowheads). The BST also showed significantly stronger connectivity with the thalamus (*magenta* arrowheads) and periaqueductal gray (*green* arrowheads). The only regions showing stronger connectivity with the Ce were neighboring regions of the amygdala (*white* arrowheads), including voxels in the region of the amygdalohippocampal area and the basolateral, basomedial, cortical, and medial nuclei. Conventions are similar to Figure 4. Note: Results are depicted here and reported in the accompanying tables for clusters of at least 80 mm^3. Abbreviations—BST, bed nucleus of the stria terminalis; Ce, central nucleus of the amygdala; L, left hemisphere; R, right hemisphere.

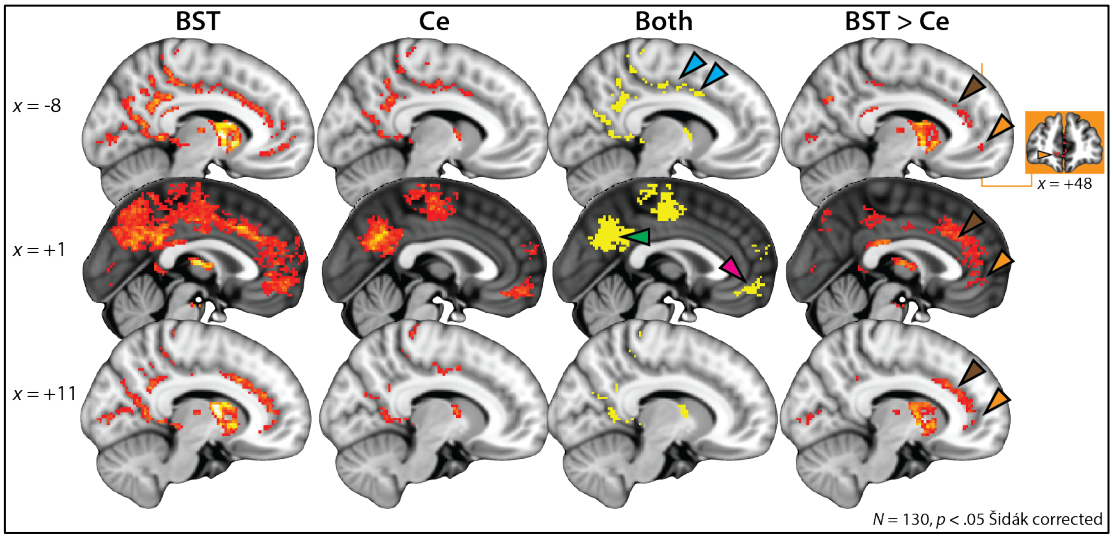

Figure 7. Cortical Regions Showing Significant Functional Connectivity with the Bed Nucleus of the Stria Terminalis (BST), Central Nucleus of the Amygdala (Ce), or Both. The first two columns depict the results of whole-brain regression analyses for the BST and Ce seed regions, respectively (p<.05, whole-brain corrected). The third column depicts the intersection (Boolean 'AND') of the two thresholded maps. The fourth column depicts the results of a paired *t*-test comparing the intrinsic functional connectivity of the BST and Ce (p<.05, small-volume corrected). Both seeds show significant functional connectivity with clusters in the posterior cingulate/precuneus (*green* arrowhead), posterior midcingulate cortex (*cyan* arrowheads), and vmPFC (*magenta* arrowhead). Relative to the Ce, the BST shows significantly stronger coupling with the anterior midcingulate and pregenual anterior cingulate cortices (*brown* arrowheads) as well as the vmPFC (*orange* arrowheads). Orange inset depicts a coronal slice through the vmPFC cluster, which extends along the rostral-caudal axis from area 10r/m and the inferior frontopolar gyrus to the rostral gyrus and pregenual anterior cingulate cortex. Conventions are similar to Figure 4 (first three columns) and Figure 6 (fourth column). Abbreviations—BST, bed nucleus of the stria terminalis; Ce, central nucleus of the amygdala; L, left hemisphere; R, right hemisphere.

Supplementary Figures

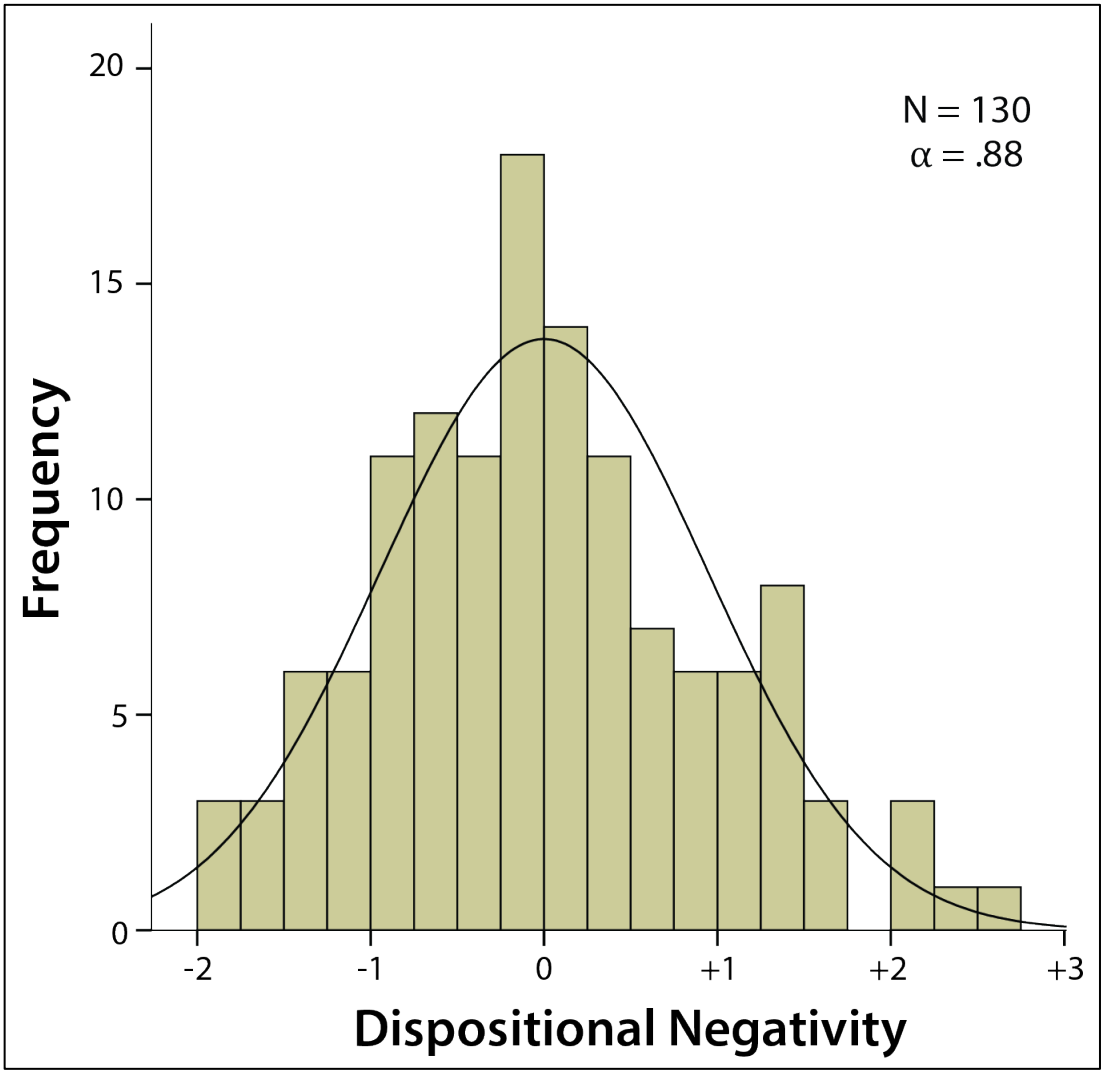

*Supplementary Figure 1. Individual differences in dispositional negativity for subjects with usable imaging data (*n *=130).* The internal-consistency reliability of the composite measure was good (α = .88).

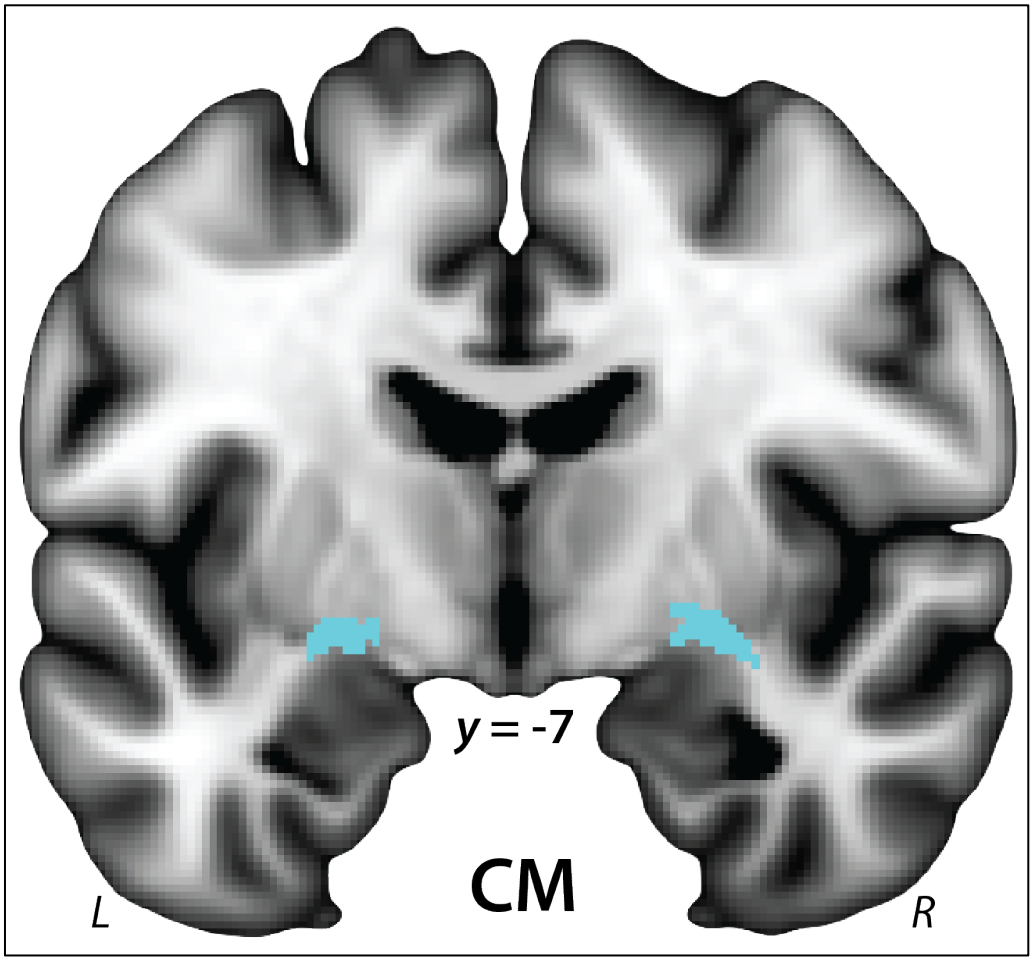

Supplementary Figure 2. Jülich Centromedial Amygdala (CM) Seeds. The derivation of the widely used probabilistic CM seed (*cyan*) is described in more detail in Amunts and colleagues (2005). This figure depicts the version of the CM seed distributed with the FSL software package thresholded at 25% and overlaid on the nonlinear MNI152 anatomical template. It is clear that the CM seeds encompass a substantial volume of extra-amygdalar tissue, including regions of white matter, globus pallidus, and putamen. A similar pattern was evident when the seeds were thresholded at 50%. For illustrative purposes, 1-mm seeds are shown. Analyses employed seeds decimated to the 2-mm resolution of the EPI data. Abbreviations—L, left hemisphere; R, right hemisphere.

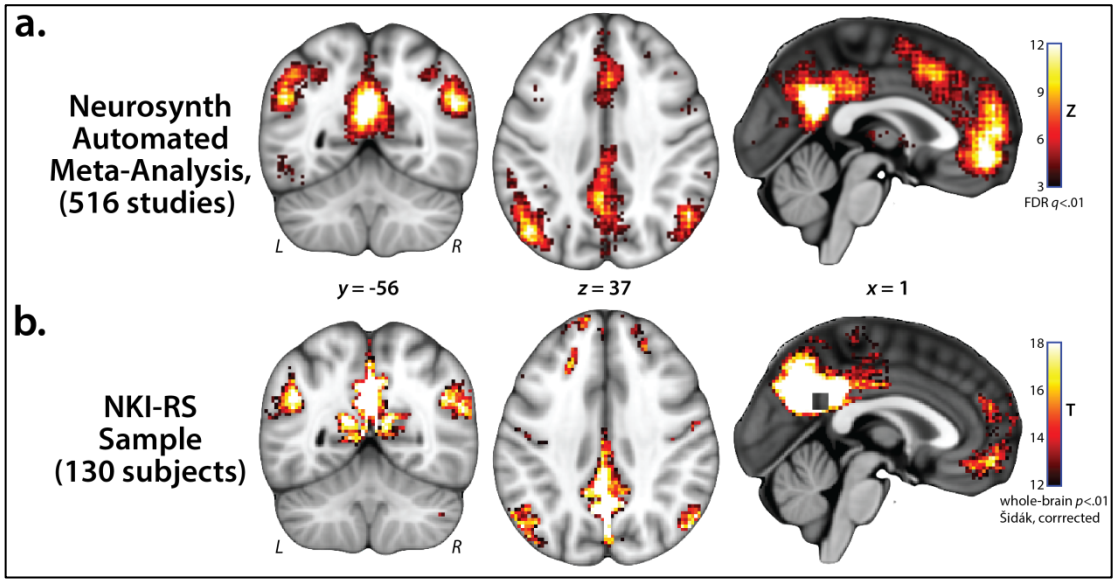

Supplementary Figure 3. Confirmatory Analysis of the Default Mode Network (DMN). For quality assurance purposes, we performed a confirmatory analysis of the DMN and compared it to an automated meta-analysis of 'default mode' performed using Neurosynth (FDR $q < .01$; Yarkoni, Poldrack, Nichols, Van Essen, & Wager, 2011). Our confirmatory analysis was performed using a 10-mm seed (square-shaped region in panel B) centered on the location ($x = 0$, $y = -50$, $z = 28$) in the precuneus showing the strongest reverse-inference association with 'default mode' in the Neurosynth database. For illustrative purposes, the resulting map was conservatively thresholded ($T > 16.0$, $p < 9.6 \times 10^{-23}$, uncorrected). As expected, both the automated meta-analysis (panel A) and confirmatory analysis (panel B) revealed regions typical of the DMN, including the posterior cingulate cortex, medial prefrontal cortex, and lateral temporoparietal cortex. Abbreviations—L, left hemisphere; R, right hemisphere.

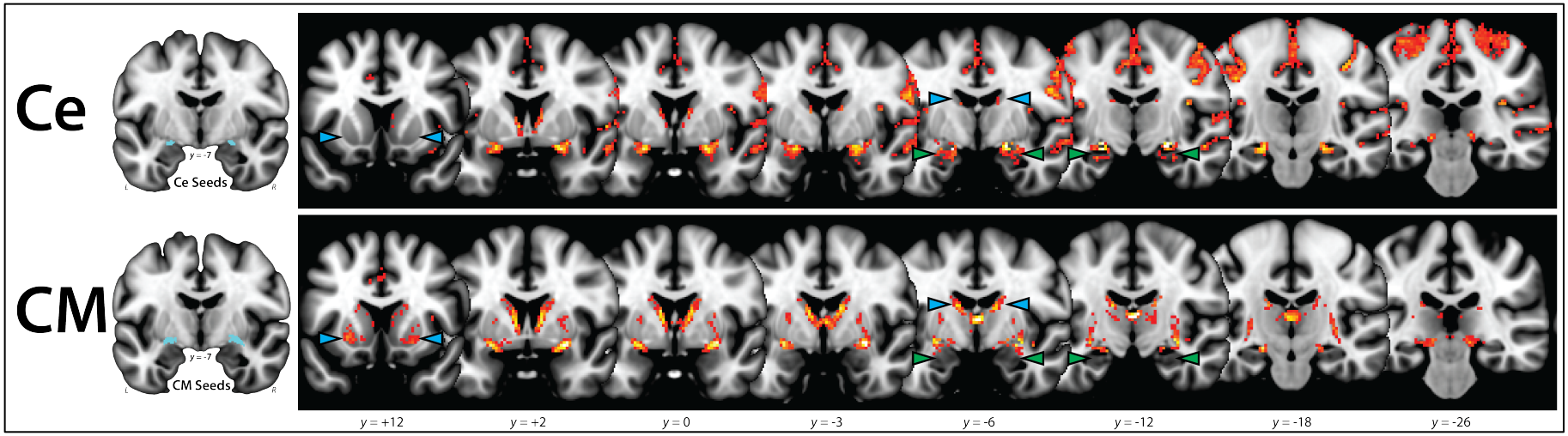

Supplementary Figure 4. Exploratory comparison of the intrinsic functional connectivity of the Ce and CM seeds. Seed regions are depicted in cyan. Black panels depict the results of whole-brain regression analyses conservatively thresholded at $p<.05$, whole-brain Šidák corrected. Qualitatively, the CM seed showed stronger coupling with the basal ganglia (caudate and putamen; *blue* arrowheads) and weaker coupling with other regions of the amygdala (*green* arrowheads) compared to the Ce seed. This pattern is consistent with the location of the CM seed, which encompasses the globus pallidus and the ventral edge of the putamen (see Supplementary Figure 2). This likely reflects a registration error when the CM seed was normalized to the MNI152 nonlinear template prior to distribution with the FSL software package (Simon Eichoff, *personal communication, 12/15/2016*). For illustrative purposes, 1-mm seeds are shown. Analyses employed seeds decimated to the 2-mm resolution of the EPI data. Conventions are similar to Figure 4. Abbreviations—Ce, central nucleus of the amygdala (seed); CM, centromedial (cytoarchitectonically defined probabilistic seed encompassing the central and medial nuclei of the amygdala). L, left hemisphere; R, right hemisphere.

References

Aggleton, J. P., & Mishkin, M. (1984). Projections of the amygdala to the thalamus in the cynomolgus monkey. *The Journal of Comparative Neurology*, *222*(1), 56–68. http://doi.org/10.1002/cne.902220106

Alheid, G. F., & Heimer, L. (1988). New perspectives in basal forebrain organization of special relevance for neuropsychiatric disorders: The striatopallidal, amygdaloid, and corticopetal components of substantia innominata. *Neuroscience*, *27,* 1–39. http://dx.doi.org/10.1016/0306- 4522(88)90217-5

Amunts, K., Kedo, O., Kindler, M., Pieperhoff, P., Mohlberg, H., Shah, N. J., ... & Zilles, K. (2005). Cytoarchitectonic mapping of the human amygdala, hippocampal region and entorhinal cortex: intersubject variability and probability maps. *Anatomy and Embryology, 210* (5-6), 343-352.

Ashburner, J. & Friston, K.J. (2005). Unified segmentation. *NeuroImage, 26,* 839–851. doi: 10.1016/j.neuroimage.2005.02.018.

Avants, B. B., Epstein, C. L., Grossman, M., & Gee, J. C. (2008). Symmetric diffeomorphic image registration with cross-correlation: evaluating automated labeling of elderly and neurodegenerative brain. *Medical Image Analysis*, 12(1), 26-41.

Avants, B., Tustison, N., Song, G., Cook, P., Klein, A., & Gee, J. (2011). A reproducible evaluation of ANTs similarity metric performance in brain image registration. *Neuroimage, 54*, 2033-2044.

Avants, B.B., Tustison, N.J., Song, G., & Gee, J.C. (2009). ANTS: Advanced Open-Source Normalization Tools for Neuroanatomy. Penn Image Computing and Science Laboratory.

Avants, B. B., Yushkevich, P., Pluta, J., Minkoff, D., Korczykowski, M., Detre, J., & Gee, J. C. (2010). The optimal template effect in hippocampus studies of diseased populations. *Neuroimage, 49*, 2457-2466.

Avery, S.N., Clauss, J.A., & Blackford, J.U. (2016). The human BNST: functional role in anxiety and addiction. *Neuropsychopharmacology, 41*(1), 126-141.

Avery, S. N., Clauss, J. A., Winder, D. G., Woodward, N., Heckers, S., & Blackford, J. U. (2014). BNST neurocircuitry in humans. *Neuroimage*, *91*, 311-323.

Bandler, R., Price, J. L., & Keay, K. A. (2000). Brain mediation of active and passive emotional coping. *Progress in Brain Research, 122,* 333-49.

Barlow, D. H., Ellard, K. K., Sauer-Zavala, S., Bullis, J. R., & Carl, J. R. (2014). The origins of neuroticism. *Perspectives on Psychological Science, 9,* 481– 496. http://dx.doi.org/10.1177/1745691614544528

Barlow, D. H., Sauer-Zavala, S., Carl, J. R., Bullis, J. R., & Ellard, K. K. (2013). The nature, diagnosis, and treatment of neuroticism: Back to the future. *Clinical Psychological Science, 2.* 344-365.

Berridge, K. C., Robinson, T. E., & Aldridge, J. W. (2009). Dissecting components of reward:'liking','wanting', and learning. *Current Opinion in Pharmacology*, *9*(1), 65-73.

Birn, R. M., Shackman, A. J., Oler, J. A., Williams, L. E., McFarlin, D. R., Rogers, G. M., . . . Kalin, N. H. (2014). Evolutionarily

conserved dysfunction of prefrontal-amygdalar connectivity in early-life anxiety. *Molecular Psychiatry,* 19, 915-922.

Biswal, B., Zerrin Yetkin, F., Haughton, V. M., & Hyde, J. S. (1995). Functional connectivity in the motor cortex of resting human brain using echo-planar MRI. *Magnetic Resonance in Medicine*, 34(4), 537-541.

Blackford, J. U., Clauss, J. A., Avery, S. N., Cowan, R. L., Benningfield, M. M., & VanDerKlok, R. M. (2014). Amygdala–cingulate intrinsic connectivity is associated with degree of social inhibition. *Biological Psychology, 99*, 15-25.

Block, J. (1995). A contrarian view of the five-factor approach to personality description. *Psychological Bulletin, 117,* 187–215. http://dx.doi .org/10.1037/0033-2909.117.2.187

Block, J. (2010). The five-factor framing of personality and beyond: Some ruminations. *Psychological Inquiry, 21,* 2–25. http://dx.doi.org/10.1080/ 10478401003596626

Buckner, R.L., Krienen, F.M., & Yeo, B.T. (2013). Opportunities and limitations of intrinsic functional connectivity MRI. *Nature Neuroscience, 16,* 832–837.

Buhle, J. T., Silvers, J. A., Wager, T. D., Lopez, R., Onyemekwu, C., Kober, H., . . . Ochsner, K. N. (2014). Cognitive reappraisal of emotion: A meta-analysis of human neuroimaging studies. *Cerebral Cortex, 24,* 2981-2990.

Bystritsky, A. (2006). Treatment-resistant anxiety disorders. *Molecular Psychiatry, 11,* 805– 814. http://dx.doi.org/10.1038/sj.mp.4001852

Calder, A. J., Ewbank, M., & Passamonti, L. (2011). Personality influences the neural responses to viewing facial expressions of emotion. *Philosophical Transactions of the Royal Society of London Series B, Biological Sciences, 366,* 1684 –1701.

Caspi, A., Roberts, B. W., & Shiner, R. L. (2005). Personality development: Stability and change. *Annual Review of Psychology, 56,* 453– 484. http://dx.doi.org/10.1146/annurev.psych.55.090902.141913

Cavanagh, J. F., & Shackman, A. J. (2015). Frontal midline theta reflects anxiety and cognitive control: Meta-analytic evidence. *Journal of Physiology, Paris*, 109, 3–15. http://dx.doi.org/10.1016/j.jphysparis.2014.04.003

Calhoon, G. G., & Tye, K. M. (2015). Resolving the neural circuits of anxiety. *Nature Neuroscience, 18,* 1394-1404.

Chronis-Tuscano, A., Rubin, K. H., O'Brien, K. A., Coplan, R. J., Thomas, S. R., Dougherty, L. R.,... Wimsatt, M. (2015). Preliminary evaluation of a multimodal early intervention program for behaviorally inhibited preschoolers. *Journal of Consulting and Clinical Psychology, 83,* 534 – 540. http://dx.doi.org/10.1037/a0039043

Clifford, S., Lemery-Chalfant, K., & Goldsmith, H. H. (2015). The unique and shared genetic and environmental contributions to fear, anger, and sadness in childhood. *Child Development*, *86*, 1538-1556.

Cox, R. (1996). AFNI: Software for Analysis and Visualization of Functional Magnetic Resonance Neuroimages, *Computers and Biomedical Research, 29,* 162–73.

Dziobek I, Bahnemann M, Convit A, & Heekeren HR. (2010). THe role of the fusiform-amygdala system in the pathophysiology of autism. *Archives of General Psychiatry*, *67*(4), 397–405. http://doi.org/10.1001/archgenpsychiatry.2010.31

Dong, H.-W., & Swanson, L. W. (2004). Organization of axonal projections from the anterolateral area of the bed nuclei of the stria terminalis. *Journal of Comparative Neurology*, *468*(2), 277–298.

Eickhoff, S.B., Stephan, K.E., Mohlberg, H., Grefkes, C., Fink, G.R., Amunts, K., & Zilles, K. (2005): A new SPM toolbox for combining probabilistic cytoarchitectonic maps and functional imaging data. *NeuroImage, 25,* 1325–1335.

Eklund, A., Nichols, T. E., & Knutsson, H. (2016). Cluster failure: Why fMRI inferences for spatial extent have inflated false-positive rates. *Proceedings of the National Academy of Sciences USA*,*113*, 7900-7905.

Ekstrom, L.B., Roelfsema, P. R., Arsenault, J. T., Bonmassar, G., & Vanduffel, W. (2008). Bottom-up dependent gating of frontal signals in early visual cortex. *Science, 321*, 414-417. doi: 10.1126/science.1153276

Entis, J. J., Doerga, P., Barrett, L. F., & Dickerson, B. C. (2012). A reliable protocol for the manual segmentation of the human amygdala and its subregions using ultra-high resolution MRI. *NeuroImage, 60,* 1226-1235.

Etkin, A., & Wager, T. D. (2007). Functional neuroimaging of anxiety: A meta-analysis of emotional processing in PTSD, social anxiety disorder, and specific phobia. *American Journal of Psychiatry, 164*, 1476-1488. http://dx.doi.org/10.1176/appi.ajp.2007.07030504

Feinstein, J. S., Adolphs, R., Damasio, A., & Tranel, D. (2011). The human amygdala and the induction and experience of fear. *Current Biology, 21,* 34 –38. http://dx.doi.org/10.1016/j.cub.2010.11.042

Feinstein, J. S., Adolphs, R., & Tranel, D. (2016). A tale of survival from the world of Patient S.M. In D. G. Amaral & R. Adolphs (Eds.), *Living without an amygdala*. New York: Guilford.

Fox, A. S. & Kalin, N. H. (2014). A translational neuroscience approach to understanding the development of social anxiety disorder and its pathophysiology. *American Journal of Psychiatry. 171),*1162–1173.

Fox, A. S., Oler, J. A., Shackman, A. J., Shelton, S. E., Raveendran, M., McKay, D. R., ... & Rogers, J. (2015a). Intergenerational neural mediators of early-life anxious temperament. *Proceedings of the National Academy of Sciences USA*, *112*(29), 9118-9122.

Fox, A. S., Oler, J. A., Shelton, S. E., Nanda, S. A., Davidson, R. J., Roseboom, P. H., & Kalin, N. H. (2012). Central amygdala nucleus (Ce) gene expression linked to increased trait-like Ce metabolism and anxious temperament in young primates. *Proceedings of the National Academy of Sciences USA, 109,* 18108 – 18113. http:// dx.doi.org/10.1073/pnas.1206723109

Fox, A. S., Oler, J. A., Tromp, P. M., Fudge, J. L., & Kalin, N. H. (2015b). Extending the amygdala in theories of threat processing. *Trends in Neurosciences, 38,* 319 – 329. http://dx.doi.org/10.1016/j.tins.2015.03 .002

Fox, A. S., Shelton, S. E., Oakes, T. R., Converse, A. K., Davidson, R. J., & Kalin, N. H. (2010). Orbitofrontal cortex lesions alter anxiety-related activity in the primate

bed nucleus of stria terminalis. *Journal of Neuroscience, 30,* 7023–7027. http://dx.doi.org/10.1523/JNEUROSCI .5952-09.2010

Fox, A. S., Shelton, S. E., Oakes, T. R., Davidson, R. J., & Kalin, N. H. (2008). Trait-like brain activity during adolescence predicts anxious temperament in primates. *Plus One, 3,* e2570. doi: 10.1371/journal.pone.0002570

Fox, M. D., Snyder, A. Z., Vincent, J. L., Corbetta, M., Van Essen, D. C., & Raichle, M. E. (2005). The human brain is intrinsically organized into dynamic, anticorrelated functional networks. *Proceedings of the National Academy of Sciences USA, 102(27),* 9673-9678.

Freese, J. L., & Amaral, D. G. (2009). Neuroanatomy of the primate amygdala. In P. J. Whalen & E. A. Phelps (Eds.), *The human amygdala* (pp. 3-42). NY: Guilford.

Gabard-Durnam, L. J., Flannery, J., Goff, B., Gee, D. G., Humphreys, K. L., Telzer, E., ... & Tottenham, N. (2014). The development of human amygdala functional connectivity at rest from 4 to 23years: A cross-sectional study. *NeuroImage, 95*, 193-207.

Greve, D. N., & Fischl, B. (2009). Accurate and robust brain image alignment using boundary-based registration. *NeuroImage, 48(1),* 63-72.

He, Y., Xu, T., Zhang, W., & Zuo, X. N. (2015). Lifespan anxiety is reflected in human amygdala cortical connectivity. *Human Brain Mapping, 37,* 1178-1193.

Honey, C.J., Sporns, O., Cammoun, L., Gigandet, X., Thiran, J.P., … Hagmann, P.(2009). Predicting human resting-state functional connectivity from structural connectivity. *Proceedings of the National Academy of Sciences USA, 106,* 2035–2040.

Hrybouski, S., Aghamohammadi-Sereshki, A., Madan, C. R., Shafer, A. T., Baron, C. A., Seres, P., ... & Malykhin, N. V. (2016). Amygdala subnuclei response and connectivity during emotional processing. *NeuroImage, 133,* 98-110.

Iglesias, J.E., Liu, C.Y., Thompson, P., & Tu, Z. (2011). Robust brain extraction across datasets and comparison with publicly available methods. *IEEE Transactions on Medical Imaging, 30(9),* 1617-1634.

Jo, H. J., Gotts, S. J., Reynolds, R. C., Bandettini, P. A., Martin, A., Cox, R. W., & Saad, Z. S. (2013). Effective preprocessing procedures virtually eliminate distance-dependent motion artifacts in resting state FMRI. *Journal of Applied Mathematics, 2013,* 9.

Johnston, J. B. (1923). Further contributions to the study of the evolution of the forebrain. *Journal of Comparative Neurology, 35*, 337–481.

Kalin, N. H., Shelton, S. E., & Davidson, R. J. (2004). The role of the central nucleus of the amygdala in mediating fear and anxiety in the primate. *Journal of Neuroscience, 24,* 5506 –5515. http://dx.doi.org/ 10.1523/JNEUROSCI.0292-04.2004

Kalin, N. H., Shelton, S. E., & Davidson, R. J. (2007). Role of the primate orbitofrontal cortex in mediating anxious temperament. *Biological Psychiatry*, *62* (10), 1134-1139.

Kalin, N. H., Fox, A. S., Kovner, R., Riedel, M. K., Fekete, E. M., Roseboom, P. H.,... Oler, J. A. (2016). Overexpressing corticotropinreleasing hormone in the primate amygdala increases anxious temperament and alters its neural circuit.

Biological Psychiatry, 80, 345–355. http://dx.doi.org/10.1016/j.biopsych.2016.01.010

Kessler, R. C., Petukhova, M., Sampson, N. A., Zaslavsky, A. M., & Wittchen, H. U. (2012). Twelve-month and lifetime prevalence and lifetime morbid risk of anxiety and mood disorders in the United States. International. *Journal of Methods in Psychiatric Research, 21,* 169 –184. http://dx.doi.org/10.1002/mpr.1359

Kim, M. J., Loucks, R. A., Palmer, A. L., Brown, A. C., Solomon, K. M., Marchante, A. N., & Whalen, P. J. (2011). The structural and functional connectivity of the amygdala: from normal emotion to pathological anxiety. *Behavioural Brain Research, 223(2),* 403-410.

Klein, A., Andersson, J., Ardekani, B. A., Ashburner, J., Avants, B., … Parsey, R. V. (2009). Evaluation of 14 nonlinear deformation algorithms applied to human brain MRI registration. *NeuroImage, 46,* 786-802.

Koob, G. F., & Volkow, N. D. (2010). Neurocircuitry of addiction. *Neuropsychopharmacology, 35* (1), 217-238.

Kotov, R., Gamez, W., Schmidt, F., & Watson, D. (2010). Linking "big" personality traits to anxiety, depressive, and substance use disorders: A meta-analysis. *Psychological Bulletin, 136,* 768 – 821. http://dx.doi.org/ 10.1037/a0020327

Krüger, O., Shiozawa, T., Kreifelts, B., Scheffler, K., & Ethofer, T. (2015). Three distinct fiber pathways of the bed nucleus of the stria terminalis to the amygdala and prefrontal cortex. *Cortex, 66*, 60-68.

LeDoux, J. E., Iwata, J., Cicchetti, P., & Reis, D. J. (1988). Different projections of the central amygdaloid nucleus mediate autonomic and behavioral correlates of conditioned fear. *The Journal of Neuroscience*, *8*(7), 2517–2529.

Lu, J., Liu, H., Zhang, M., Wang, D., Cao, Y., Ma, Q., …Li, K. (2011). The intrinsic functional connectivity reflects polysnaptic anatomical pathways. *Journal of Neuroscience, 31*, 15065-15071.

Mai, J. K., Paxinos, G., & Voss, T. (2007): *Atlas of the Human Brain*, 3rd ed. San Diego, CA: Academic Press.

Maren, S., Phan, K. L., & Liberzon, I. (2013). The contextual brain: implications for fear conditioning, extinction and psychopathology. *Nature Reviews Neuroscience*, *14*(6), 417–428. http://doi.org/10.1038/nrn3492

Marusak, H. A., Thomason, M. E., Peters, C., Zundel, C., Elrahal, F., & Rabinak, C. A. (2016). You say 'prefrontal cortex'and I say 'anterior cingulate': meta-analysis of spatial overlap in amygdala-to-prefrontal connectivity and internalizing symptomology. *Translational Psychiatry*, *6*(11), e944.

Mayberg, H. S. (1997). Limbic-cortical dysregulation: a proposed model of depression. *The Journal of Neuropsychiatry and Clinical Neurosciences*, *9,* 471-481.

McCrae, R. R. & Costa, P. T. (2004). A contemplated revision of the NEO Five-Factor Inventory. *Personality and Individual Differences, 36,* 587-596.

Moffitt, T. E., Poulton, R., & Caspi, A. (2013). Lifelong impact of early self-control. *American Scientist, 101*, 352–359. http://dx.doi.org/10 .1511/2013.104.352

Morey, R. A., Dolcos, F., Petty, C. M., Cooper, D. A., Hayes, J. P., … McCarthy, G. (2009). The role of trauma-related distractors on neural systems for working memory and emotion processing in post traumatic stress disorder. *Journal of Psychiatry Research, 43* (8), 809-817.

Motzkin, J. C., Philippi, C. L., Oler, J. A., Kalin, N. H., Baskaya, M. K., & Koenigs, M. (2015). Ventromedial prefrontal cortex damage alters resting blood flow to the bed nucleus of stria terminalis. *Cortex*, *64*, 281-288.

Münsterkötter, A. L., Notzon, S., Redlich, R., Grotegerd, D., Dohm, K., Arolt, V.,... Dannlowski, U. (2015). Spider or no spider? Neural correlates of sustained and phasic fear in spider phobia. *Depression and Anxiety, 32,* 656 – 663. http://dx.doi.org/10.1002/da.22382

Nacewicz, B. M., Alexander, A. L., Kalin, N. H. & Davidson, R. J. (2014). The neurochemical underpinnings of human amygdala volume including subregional contributions. *Biological Psychiatry, 75,* S222.

Nashold, B. S., Wilson, W. P., & Slaughter, D. G. (1969). Sensations evoked by stimulation in the midbrain of man. *Journal of Neurosurgery, 30*, 14–24.

Nichols, T., Brett, M., Andersson, J., Wager, T., & Poline, J. B. (2005). Valid conjunction inference with the minimum statistic. *NeuroImage, 25*, 653-660.

Nauta, W. J. (1961). Fibre degeneration following lesions of the amygdaloid complex in the monkey. *Journal of Anatomy, 95*, 515–531.

Nooner, K.B., Colcombe, S.J., Tobe, R.H., Mennes, M., Benedict, M.M., … Milham M. P. (2012). The NKI-Rockland Sample: a model for accelerating the pace of discovery science in psychiatry. *Frontiers in Neuroscience, 6,* 152.

Oler, J. A., Birn, R. M., Patriat, R., Fox, A. S., Shelton, S. E., Burghy, C. A., ... & Kalin, N. H. (2012). Evidence for coordinated functional activity within the extended amygdala of non-human and human primates. *NeuroImage, 61(4),* 1059-1066.

Ongur, D., Ferry, A. T., & Price, J. L. (2003). Architectonic subdivision of the human orbital and medial prefrontal cortex. *Journal of Comparative Neurology, 460*, 425-449.

Ormel, J., Jeronimus, B. F., Kotov, R., Riese, H., Bos, E. H., Hankin, B., . . . Oldehinkel, A. J. (2013). Neuroticism and common mental disorders: Meaning and utility of a complex relationship. *Clinical Psychology Review, 33,* 686 – 697. http://dx.doi.org/10.1016/j.cpr.2013.04.003

Oler, J. A., Tromp, D. P., Fox, A. S., Kovner, R., Davidson, R. J., Alexander, A. L., . . . Fudge, J. L. (*2016*). Connectivity between the central nucleus of the amygdala and the bed nucleus of the stria terminalis in the non-human primate: neuronal tract tracing and developmental neuroimaging studies. *Brain Structure and Funct*ion

Pessoa, L. (2013). *The cognitive-emotional brain: From interactions to integration.* Cambridge, MA: MIT Press.

Pizzagalli, D. A. (2011). Frontocingulate dysfunction in depression: toward biomarkers of treatment response. *Neuropsychopharmacology*, *36*(1), 183-206.

Power, J. D., Schlaggar, B. L., & Petersen, S. E. (2015). Recent progress and outstanding issues in motion correction in resting state fMRI. *NeuroImage,105,* 536-551.

Prevost, C., McCabe, J. A., Jessup, R. K., Bossaerts, P., & O'Doherty, J. P. (2011). Differentiable contributions of human amygdalar subregions in the computations underlying reward and avoidance learning. *European Journal of Neuroscience, 34(1),* 134-145.

Quirk, G. J., & Gehlert, D. R. (2003). Inhibition of the amygdala: key to pathological states?. *Annals of the New York Academy of Sciences*, *985*(1), 263-272.

Roy, A. K., Benson, B. E., Degnan, K. A., Perez-Edgar, K., Pine, D. S., Fox, N. A., & Ernst, M. (2014). Alterations in amygdala functional connectivity reflect early temperament. *Biological Psychology, 103,* 248-254.

Roy, A. K., Fudge, J. L., Kelly, C., Perry, J. S., Daniele, T., Carlisi, C., ... & Ernst, M. (2013). Intrinsic functional connectivity of amygdala-based networks in adolescent generalized anxiety disorder. *Journal of the American Academy of Child & Adolescent Psychiatry*, *52*(3), 290-299.

Roy, A. K., Shehzad, Z., Margulies, D. S., Kelly, A. C., Uddin, L. Q., Gotimer, K., ... & Milham, M. P. (2009). Functional connectivity of the human amygdala using resting state fMRI. *Neuroimage*, *45*(2), 614-626.

Satpute, A. B., Wager, T. D., Cohen-Adad, J., Bianciardi, M., Choi, J. K., Buhle, J. T., . . . Barrett, L. F. (2013). Identification of discrete functional subregions of the human periaqueductal gray. *Proceedings of the National Academy of Sciences USA, 110,* 17101-17106.

Schuyler, B. S., Kral, T. R., Jacquart, J., Burghy, C. A., Weng, H. Y., Perlman, D. M.,... Davidson, R. J. (2014). Temporal dynamics of emotional responding: Amygdala recovery predicts emotional traits. *Social Cognitive and Affective Neuroscience, 9,* 176 –181. http://dx.doi .org/10.1093/scan/nss131

Shattuck, D. W., Sandor-Leahy, S. R., Schaper, K. A., Rottenberg, D. A., & Leahy, R. M. (2001). Magnetic resonance image tissue classification using a partial volume model. *NeuroImage, 13*, 856-876.

Shackman, A. J., Kaplan, C. M., Stockbridge, M. D., Tillman, R. M., Tromp, D. P. M., Fox, A. S., & Gamer, M. (2016b). The neurobiology of anxiety and attentional biases to threat: Implications for understanding anxiety disorders in adults and youth. *Journal of Experimental Psychopathology, 7*, 311-342.

Shackman, A. J., & Fox, A. S. (2016). Contributions of the central extended amygdala to fear and anxiety. *Journal of Neuroscience, 36*, 8050 – 8063.

Shackman, A. J., Fox, A. S., Oler, J. A., Shelton, S. E., Oakes, T. R., Davidson, R. J., & Kalin, N. H. (*in press*). Heightened extended amygdala metabolism following threat characterizes the early phenotypic risk to develop anxiety-related psychopathology. *Molecular Psychiatry*.

Shackman, A. J., Fox, A. S., Oler, J. A., Shelton, S. E., Davidson, R. J., & Kalin, N. H. (2013). Neural mechanisms underlying heterogeneity in the presentation of anxious temperament. *Proceedings of the National Academy of Sciences USA, 110,* 6145-6150.

Shackman, A. J., Fox, A. S., & Seminowicz, D. A. (2015). The cognitive-emotional brain: Opportunities and challenges for understanding neuropsychiatric disorders. *Behavioral and Brain Sciences, 38*, e86.

Shackman, A. J., Salomons, T. V., Slagter, H. A., Fox, A. S., Winter, J. J., & Davidson, R. J. (2011). The integration of negative affect, pain and cognitive control in the cingulate cortex. *Nature Reviews Neuroscience, 12,* 154-167.

Shackman, A. J., Tromp, D. P. M., Stockbridge, M. D., Kaplan, C. M., Tillman, R. M., & Fox, A. S. (2016a). Dispositional negativity: An integrative psychological and neurobiological perspective. *Psychological Bulletin, 142,* 1275-1314 .

Siegel, J. S., Power, J. D., Dubis, J. W., Vogel, A. C., Church, J. A., Schlaggar, B. L., & Petersen, S. E. (2014). Statistical improvements in functional magnetic resonance imaging analyses produced by censoring high-motion data points. *Human Brain Mapping, 35(5),* 1981-1996.

Smith, S. M. (2002). Fast robust automated brain extraction. *Human Brain Mapping, 17(3),* 143-155.

Somerville, L. H., Whalen, P. J., & Kelley, W. M. (2010). Human bed nucleus of the stria terminalis indexes hypervigilant threat monitoring. *Biological Psychiatry, 68,* 416 – 424. http://dx.doi.org/10.1016/j.biopsych.2010.04.002

Spielberger, C. D., Gorsuch, R. L., Lushene, R., Vagg, P. R., & Jacobs, G. A. (1983). *Manual for the State-Trait Anxiety Inventory*. Palo Alto, CA: Consulting Psychologists Press.

Stelzer, J., Lohmann, G., Mueller, K., Buschmann, T., & Turner, R. (2014). Deficient approaches to human neuroimaging. *Frontiers in Human Neuroscience*, *8*, 462.

Stocker, T. (2007). On the asymptotic bias of OLS in dynamic regression models with autocorrelated errors. *Statistical Papers, 48(1),* 81-93.

Theiss, J. D., Ridgewell, C., McHugo, M., Heckers, S., & Blackford, J. U. (2016). Manual segmentation of the human bed nucleus of the stria terminalis using 3T MRI. *NeuroImage, 146*, 288-292.

Torrisi, S., O'Connell, K., Davis, A., Reynolds, R., Balderston, N., … Ernst, M. (2015). Resting state connectivity of the bed nucleus of the stria terminalis at ultra-high field. *Human Brain Mapping, 36*, 4076-4088. doi: 10.1002/hbm.22899.

Tranel, D., Gullickson, G., Koch, M., & Adolphs, R. (2006). Altered experience of emotion following bilateral amygdala damage. *Cognitive Neuropsychiatry, 11,* 219 –232. http://dx.doi.org/10.1080/13546800444000281

Turner, R., & Geyer, S. (2014). Comparing like with like: the power of knowing where you are. *Brain Connectivity*, *4*(7), 547-557.

Tustison, N. J., Cook, P. A., Klein, A., Song, G., Das, S. R., Duda, J. T., ... & Avants, B. B. (2014). Large-scale evaluation of ANTs and FreeSurfer cortical thickness measurements. *NeuroImage, 99,* 166-179.

Tyler, L. K., Chiu, S., Zhuang, J., Randall, B., Devereux, B. J., Wright, P., … Taylor, K. I. (2013). Objects and Categories: Feature Statistics and Object Processing in the Ventral Stream. *Journal of Cognitive Neuroscience*, *25*(10), 1723–1735. http://doi.org/10.1162/jocn_a_00419

Tyszka, J. M., & Pauli, W. M. (2016). In vivo delineation of subdivisions of the human amygdaloid complex in a high-resolution group template. *Human Brain Mapping, 37*, 3979-3998.

Vincent, J.L., Patel, G.H., Fox, M.D., Snyder, A.Z., Baker, J.T., … Raichle, M.E. (2007). Intrinsic functional architecture in the anaesthetized monkey brain. *Nature, 447*, 83–86.

Walker, D. L., Toufexis, D. J., & Davis, M. (2003). Role of the bed nucleus of the stria terminalis versus the amygdala in fear, stress, and anxiety. *European Journal of Pharmacology*, *463*(1), 199-216.

Whalen, P. J., Johnstone, T., Somerville, L. H., Nitschke, J. B., Polis, S., Alexander, A. L., ... & Kalin, N. H. (2008). A functional magnetic resonance imaging predictor of treatment response to venlafaxine in generalized anxiety disorder. *Biological psychiatry*, *63*(9), 858-863.

Whiteford, H. A., Degenhardt, L., Rehm, J., Baxter, A. J., Ferrari, A. J., Erskine, H. E.,... Vos, T. (2013). Global burden of disease attributable to mental and substance use disorders: Findings from the Global Burden of Disease Study 2010. *Lancet, 382,* 1575–1586. http://dx.doi.org/10 .1016/S0140-6736(13)61611-6

Yarkoni, T., Poldrack, R. A., Nichols, T. E., Van Essen, D. C., & Wager, T. D. (2011). Large-scale automated synthesis of human functional neuroimaging data. *Nature Methods, 8*, 665-670.

Yassa, M. A., Hazlett, R. L., Stark, C. E., & Hoehn-Saric, R. (2012). Functional MRI of the amygdala and bed nucleus of the stria terminalis during conditions of uncertainty in generalized anxiety disorder. *Journal of Psychiatric Research, 46,* 1045–1052. http://dx.doi.org/10.1016/j .jpsychires.2012.04.013

Yilmazer-Hanke, D. M. (2012). Amygdala. In J. K. Mai & G. Paxinos (Eds.), *The human nervous system* (pp. 759–834). San Diego, CA: Academic Press.

Zinbarg, R. E., Mineka, S., Bobova, L., Craske, M. G., Vrshek-Schallhorn, S., Griffith, J. W., . . . Anand, D. (2016). Testing a hierarchical model of neuroticism and its cognitive facets: Latent structure and prospective prediction of first onsets of anxiety and unipolar mood disorders during 3 years in late adolescence. *Clinical Psychological Science, 4,* 805-824.